UNIVERSITY OF OTTAWA

A STUDY OF THE CHARGED π-MESON DISTRIBUTION FROM THE INELASTIC COLLISION OF 6.2 BEV PROTONS WITH EMULSION NUCLEI

by

Sheung Tsing Lam

Submitted in partial fulfillment
of the requirements for the degree of
Master of Science.

Department of Physics,
Faculty of Pure and Applied Science
The University of Ottawa,
Ottawa, Canada

May 1962

ABSTRACT

The inelastic collision between 6.2 Bev protons and emulsion nuclei is studied. The interaction with C, N and O forms the light group, while that with Ag and Br forms the heavy group. The analysis of the angular distribution of the charged π-mesons produced indicates that the incident protons interact with different target masses as they traverse the target nuclei. Also the interaction between the incident proton and the meson field of the nucleon situated at the edge of the target nucleus is observed. The angular distribution of the charged π-mesons in the centre of mass system is isotropic for the interaction where three, four or five target nucleon masses are involved. However, in the cases when one target nucleon mass is involved and when the interaction occurs with the meson field of the peripheral nucleons, the angular distribution in the centre of mass system does not show spherical symmetry. The study of the transverse momentum and the energy distributions of the charged π-mesons also indicates the presence of the interaction between the incident proton and the meson field of the peripheral nucleons of the target nucleus.

ACKNOWLEDGEMENT

I would like to express my gratitude to my Supervisor, Mr. Jacques Hébert, for his suggestion of the interesting research problem and his able guidance throughout.

I would also like to thank Mr. J. Lefaivre, and my student colleagues, especially Mr. K. Crouch and Mr. J. Ancsin, for their interest in this work and for their helpful discussions.

I am also grateful to the National Research Council Cosmic Ray Group for supplying the emulsion plates.

Financial assistance through a National Research Council grant is also gratefully acknowledged.

LIST OF FIGURES

CONTENT

1. INTRODUCTION

In a high energy nucleon-nucleon collision, the energy available in the centre of mass (C. M.) system is released in a small volume having the dimensions of the order of magnitude of the meson cloud surrounding the nucleons.(1) This volume is assumed to be:

$$V_o = \frac{4}{3}\pi R^3$$

where $R \sim \frac{\hbar}{\mu c}$ and μ = π-meson rest mass,

But in high energy interactions, the volume is subject to Lorentz contraction and hence the volume will be:

$$V = \left(\frac{2Mc^2}{W}\right) V_o$$

where M = nucleon rest mass

and W = total energy of the two colliding nucleons in the C. M. system.

Since the interactions of the meson field are strong, the energy will be distributed rapidly among the various degrees of freedom present in the volume according to statistical laws, and the probability that a certain number of mesons will be created, can be computed.

In the interaction of high energy protons with emulsion nuclei, two different models have been used to explain the production of showers, which are composed of high energy protons and charged mesons. In the statistical model, (1, 2) the incident proton sets up a cascade in the target nucleus and the consecutive collisions among the nucleons give rise to the production of a shower. However, in the tunnel model (3), the incident proton, if its energy is higher than 16 Bev, (4) punches a cylindrical tunnel in the target nucleus, and so a chunk of nucleons is

pushed out. It is the interaction between the incident proton and these nucleons that gives rise to the production of a shower. At lower energies, this tunnel may broaden towards the end and a funnel-shaped tunnel may result. This means that more nucleons are involved and theenergy available in the C. M. systen will be increased. Hence, the shower multiplicity will be higher than that for a cylindrical tunnel.

When the incident proton tunnels through the nucleus, some energy is given to the nucleus. Hence the residual nucleus is unstable and low energy nucleons and light fragments are emitted. This evaporation of the residual nucleus[5] occurs after the formation of theshower and hence these two processes can be treated distinctly from each other. The evaporation process is now being studied by K. Crouch in this laboratory.

The interaction between high energy protons and emulsion nuclei has been investigated by a number of experimenters[6-14]. Ali et al.[12] and Ancsin[13] studied the interaction with 6.2 Bev protons and found that the angular distribution of the charged mesons was isotropic in the C. M. system, although they disagreed about the different average target masses involved. Kalbach et al.[6] and Daniel et al.[9] studied the inelastic collision between 6.2 Bev protons and single nucleons (hydrogen atoms and peripheral nucleons) in the emulsion and found that the charged meson angular distribution showed forward and backward peaking in the C. M. system. In the study of 9 Bev proton interactions with emulsion nuclei, Friedländer[7] showed that there were different target masses involved in the interaction, depending on the

length or size of tunnel produced by the proton traversing the target nucleus. Barbaro-Galtieri et al.[14] also showed similar results in the study of the interaction between 27 Bev protons and emulsion nuclei.

2. CLASSIFICATION OF NUCLEAR EVENTS

A stack of Ilford G5 emulsions (14 cm x 10 cm x 0.06 cm each) was exposed to a 6.2 Bev proton beam from the Berkeley Bevatron. The method of area scanning was adopted to find nuclear events. The interactions were divided into two groups: the light group (C. N. O.) and the heavy group (Ag, Br). Stars with eight black tracks or more, which were due to the interaction of the incident proton with the heavy nuclei, were taken as big stars, while those having less than eight black tracks were taken as small stars. Tracks with normalized grain density, $g/g_0 \leqslant 2.0$, where g_0 is the grain density at the plateau ionization, were taken as shower tracks, while those with $g/g_0 > 2.0$ were taken as black tracks. Black tracks of range less than 10 microns were taken as recoils[15], which might be due to heavy evaporation fragments. So for the interaction with the light group, small stars were only those without a recoil.

3. IDENTIFICATION OF PARTICLES

A charged particle moving through matter loses its energy mainly by ionizing and exciting the atoms of the medium. If the velocity of the particle is much greater than the velocities of the

orbital electrons, the electrons can be considered as stationary relative to the incoming particle. Using this assumption, the loss of energy per unit length is arrived at by the Bohr formula:

$$-\frac{dE}{dx} = a\frac{Z^2}{E}\ln bE \qquad (3.1)$$

where E = kinetic energy of the incoming particle

Z = number of electronic charges carried by the charged particle

and, a and b are constants

But in the case with emulsion, as the charged particle moves through the emulsion, latent images will be formed in the grains of silver bromide, which have been traversed by the charged particle. If the latent image is sufficiently large, it will show as a black grain in the emulsion after development. Assuming a linear relationship between the loss of energy per unit length and the average size of latent images produced, one can show that the loss of energy per unit length is directly proportional to the grain density of the track. (This is true up to $g=4g_o$). For practical purposes, the normalized grain density, g^*, is used. It is defined as $g^* = g/g_o$, where g is the grain density of the track and g_o, which is constant, is the grain density at the plateau ionization. (See fig.1). The kinetic energy, E, is also related to the quantity, $p\beta$, where p is the momentum and β is the ratio of the velocity of the particle to the velocity of light. Hence a graph of g^* against $p\beta$ can be drawn according to equation (3.1). Fig. 1 shows the theoretical curves for charged

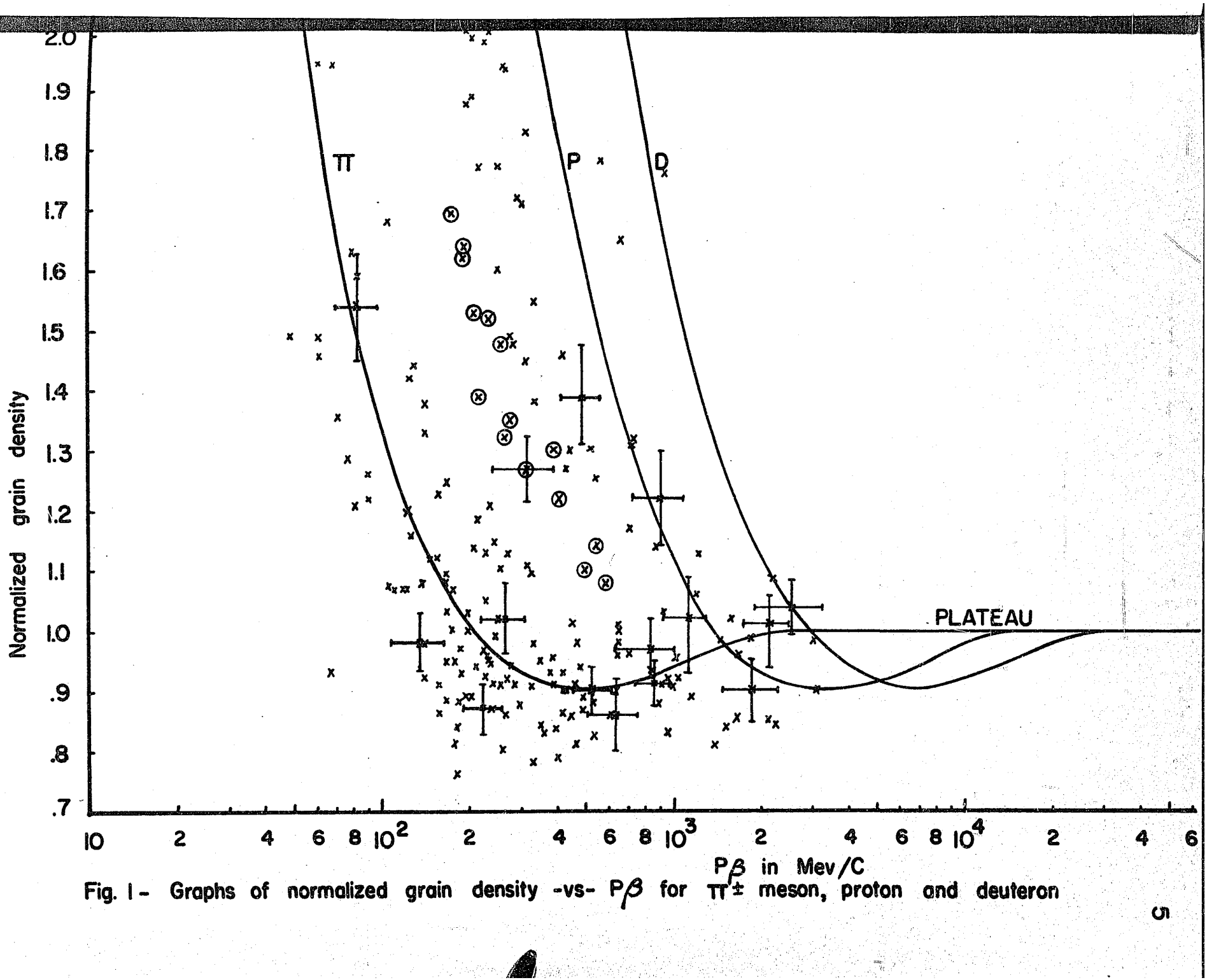

Fig. 1 - Graphs of normalized grain density -vs- $P\beta$ for $\pi^{\pm}$ meson, proton and deuteron

π-meson, proton and deuteron and the crosses are experimental points. For some points, the statistical errors are shown. This is to show the order of magnitude of the errors. Thus using this method the shower particles can be identified as protons or charged π-mesons. (We neglect the K-mesons because of their very small number).

In Fig. 1, the experimental points from the charged π-meson tracks were quite close to the theoretical curve, while those for the proton tracks were shifted to the left of the theoretical curve, with some lying quite close to it. Those lying close to the curve were found to be flat tracks and those shifted to the left were at an angle of dip more than 5°. While carrying out measurements in these tracks, the vertical motion of the microscope must be adjusted constantly to keep the track in view. This introduced a noise and hence the $p\beta$ of the track was reduced accordingly. This accounts for the shift of the experimental points to the left of the theoretical curve.

Among the shower tracks, those for which $p\beta$ was higher than 700 Mev/c could not be identified as protons or π-mesons by means of the curves shown in Fig.1, since the curves are too close. These tracks were classified as high energy tracks, emitted within a cone of 15° relative to the incident proton. Also some tracks had values of $p\beta$ and g^{*} lying in the region between the proton and the π-meson curves, where identification could not be made. These tracks were of $p\beta$ less than 700 Mev/c and were classified as unidentified tracks, some of these tracks might be charged K-mesons but it was not possible to tell definitely. These tracks were shown by the symbol ⊗ in Fig. 1.

4. MULTIPLE SCATTERING MEASUREMENT

For small scattering angles, Rutherford's formula can be written as:

$$p\beta = \frac{K(t)}{\bar{D}} \qquad - - - (4.1)$$

where $\bar{D}$ = mean scattering angle

$K(t) = .001745 \times (t)^{\frac{1}{2}} \times k$

t = cell length in microns

and $k = 24$ Mev degree/(100 microns)$^{\frac{1}{2}}$ (See reference 16)

If $\bar{D}$ is known, $p\beta$ can be found from equation (4.1), and its unit is in Mev/c.

In order to measure $\bar{D}$, a high precision stage microscope* was used, with a magnification of 100x, 12.5x. The track was aligned as parallel as possible to the direction of motion of the stage and was moved along this direction. At equal intervals t microns apart (t = cell length, see Fig.2) the deviations $y_1, y_2, \ldots y_i, \ldots$ of the track from a reference straight line were measured by means of a micrometer which formed part of the eye-piece in the microscope.

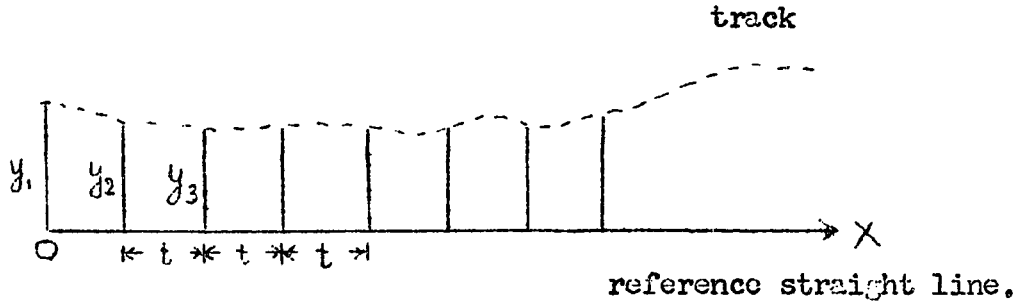

Fig. 2

*The microscope stage was built by Mr. J. Ancsin as part of his M. Sc. work in the University of Ottawa.

The angle the first segment makes with the reference line is

$$\theta_1 = \frac{y_1 - y_1}{t} \quad \text{for small angles}$$

Similarly for the second segment:

$$\theta_2 = \frac{y_2 - y_2}{t}$$

Then the magnitude of the angle between these two segments is given by:

$$|D_1| = \left|\left(\frac{y_3 - y_2}{t}\right) - \left(\frac{y_2 - y_1}{t}\right)\right|$$

Similarly, for the other segments, we have:

$$|D_2| = \left|\left(\frac{y_4 - y_3}{t}\right) - \left(\frac{y_3 - y_2}{t}\right)\right|$$

$$|D_3| = \left|\left(\frac{y_5 - y_4}{t}\right) - \left(\frac{y_4 - y_3}{t}\right)\right| \quad \text{and so on.}$$

Hence, the average value of $|D|$ gives the mean scattering angle $\bar{D}$.

The choice of a cell length is arbitrary, but the mean scattering angle of the track must be larger than the mean scattering angle due to the grain noise, which is the scattering of the emulsion grains even if the path of the charged particle is a perfect straight line. The statistical error associated with β found this way is taken as $\frac{75}{\sqrt{N}}$ percent, where N is the number of measurements.

5. GRAIN COUNTING

The grain density along the incoming proton tracks and shower tracks was found by counting grains over equal intervals along the tracks. Since $p\beta$ of the incoming proton could be measured, the normalized grain density was read off from the proton curve in Fig. 1, and hence the grain density corresponding to the plateau region was given by dividing the grain density along the incoming proton track by this value. Knowing the grain density at the plateau region, the normalized grain density of each shower track could be found. The statistical error for the grain count was taken as $\frac{1}{\sqrt{N}}$ 100 percent, where N was the total number of grains counted.

6. ANGULAR DISTRIBUTION OF STEEP TRACKS

Since the thickness of the emulsion was only 600 microns, shower particles emitted at large angles might be too steep to allow any reliable measurements, as the track in the emulsion was short. Any track which was less than 700 microns was considered to be a steep track. Assuming that the distribution of the fast protons and charged π-mesons in the steep shower tracks was the same as in the identified shower tracks, the number of charged π-meson from steep tracks could be found. The angle of emission of each identified charged π-meson was measured with respect to the direction of the incident proton. However to obtain the angular distribution of all the charged π-mesons produced, the angular distribution of the steep charged π-mesons must be taken into consideration. The following method was used for this purpose.

There are two factors which must be considered in this respect. The first one is purely geometrical. It is obvious that the larger the angle the track makes with the primary, the more probable it is that it will be less than 700 microns long in the same plate. Therefore in this correction the number of steep tracks should increase with increasing angles. But on the other hand, experiment shows that the number of charged π-meson decreases as the angle of the emission increases. Hence the angular distribution of the steep charged π-mesons must lie somewhere between these two distributions and a distribution which is the addition of the two effects is used.

First of all consider a two dimensional figures as shown in Fig. 3. Suppose O is the centre of an emulsion star and OX is the direction of the incident proton. HK is the upper surface of the emulsion. Then if OA is equal to 700 microns, i.e. the radius of the circle, any track lying at an angle greater than α will be less than 700 microns and is considered to be a steep track. OB is one of these tracks. Now let us transfer this idea into a three dimensional picture (Fig. 4), which is the true picture in nuclear emulsion. Instead of a circle, a sphere is considered; and the upper surface of the emulsion is represented by the plane HKL. Let the radius of the sphere be r (chosen to be 700 microns). Tracks making an angle θ with OX will subtend a cone of semi-apex angle θ with base CBDG. It is seen from the figure that part of these tracks forming the surface of the cone is cut off by the plane LKCEDH. OC and OD are the tracks at the limit, i.e. their length in the emulsion is just 700 microns. So these tracks (forming the surface of the cone) lying above OC and OD are taken as steep tracks. Assuming spherical symmetry for all tracks, the number of these tracks going out through a certain part of the sphere will

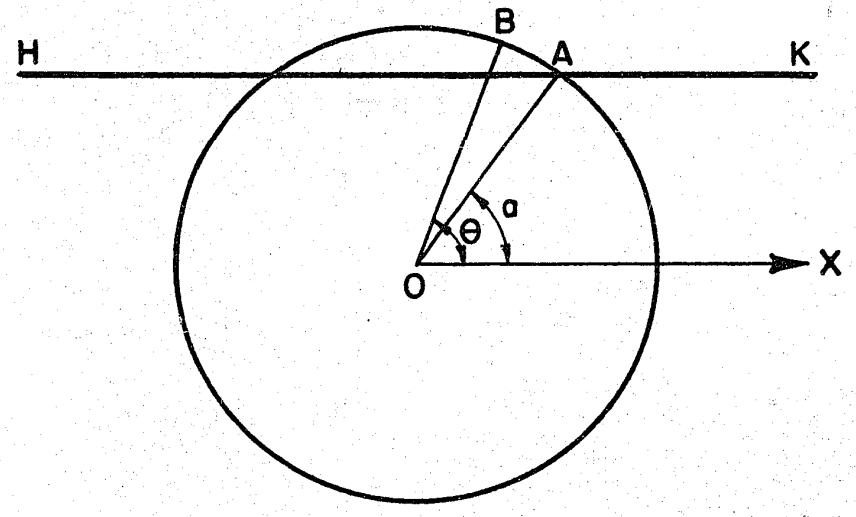

Fig. 3

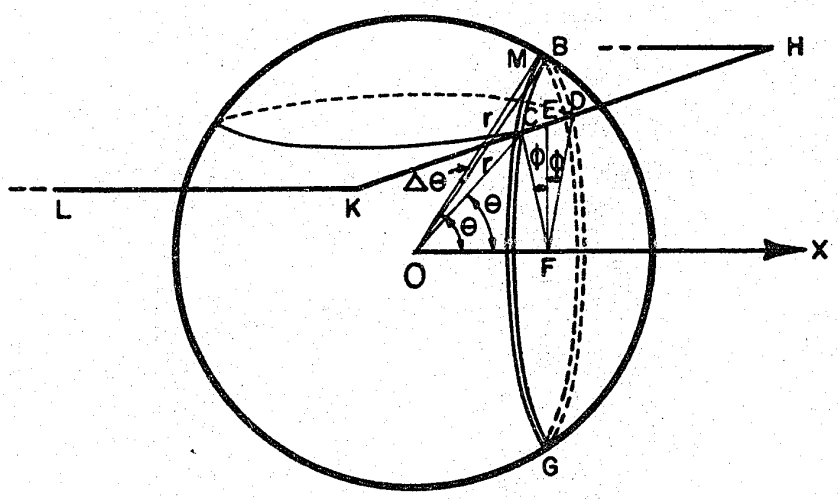

Fig. 4

just be proportional to the area of the surface. Now let us return to the section as shown in the diagram. OM is a track making an angle of $\theta + \Delta\theta$ with OX. So the area of the annular surface will be given by:

$$\Delta S = 2\pi r^2 \sin\theta \Delta\theta$$

Part of the surface area is cut off by the plane LKCEDH. In order to find the area cut off, the section CBDG, which is a circle with centre F, must be considered. As seen from the diagram, the arc CBD of the circle is cut off by the line CED. So tracks originating from O and passing through this arc will be taken as steep tracks. Now let us . find the radius of this circle. FC and FD are two of the radii:

Since $\angle OFC = 90^\circ$

$$FC = OC \sin\theta$$

$$= r \sin\theta$$

Let the perpendicular distance, FE, from the upper surface of the emulsion to the direction of the incident proton be h.

Then $\cos\phi = \frac{FE}{FC}$, since $\angle FEC = 90^\circ$

$$= \frac{h}{r \sin\theta}$$

$$\phi = \cos^{-1}\left(\frac{h}{r \sin\theta}\right)$$

The area Δa of the annular surface cut off by this plane is

$$\Delta a = \frac{2\phi}{\pi} \cdot \frac{\Delta S}{2} = \frac{\phi}{\pi} \Delta S$$

(N.B. Only the upper half of the annular surface is considered, since the lower half of the sphere must be considered with another plane

corresponding to the bottom of the emulsion).

Or in other words, the number of the steep tracks at an angle ϕ with the incident proton is:

$$\Delta f = A \frac{\phi}{\pi} \Delta S$$

Where A is a proportionality constant

$$\Delta f = \frac{A \cos^{-1}\left(\frac{h}{r \sin\theta}\right)}{\pi} \cdot 2\pi r^2 \sin\theta \Delta\theta$$

$$= 2A r^2 \sin\theta \cos^{-1}\left(\frac{h}{r\sin\theta}\right) \Delta\theta$$

Using the same argument, the number of steep tracks cut off by the bottom surface of the emulsion can also be found.

For practical purposes the various values of θ were taken at intervals of 10° (i.e. $\theta = 0^\circ, 10^\circ, 20^\circ$, and so on). So the annular surface area between angles θ_1 and θ_2 will be:

$$S = \int dS$$

$$= 2\pi r^2 \int_{\theta_1}^{\theta_2} \sin\theta \, d\theta$$

$$= 2\pi r^2 (\cos\theta_1 - \cos\theta_2)$$

Therefore, the number of steep tracks lying between the angles θ_1 and θ_2 is:

$$\Delta f_{\theta_1 \theta_2} = 2A r^2 (\cos\theta_1 - \cos\theta_2) \cos^{-1}\left(\frac{h}{r\sin\theta}\right) \quad \text{--------} \quad (6.2)$$

where $\theta = \frac{\theta_1 + \theta_2}{2}$

As seen from equation (6.2) $\Delta F_{\theta_1\theta_2}$ depends on h, which is the depth of the emulsion star. In the selection of stars, only those lying between 100 microns and 500 microns from the upper surface of the emulsion were used. So h in this case varied from 100 microns to 500 microns. For practical purposes h was chosen in steps of 100 microns (i.e. h = 100, 200, ..., 500 microns). For different values of h, $\Delta f_{\theta_1\theta_2}$ was calculated and all these were added to give the total number of steep tracks. So the fractions of steep tracks lying at different angle intervals were found. This distribution was plotted as shown in Figs. 5 and 6 (curve A). Hence using this method the effect of the geometrical factor on the angular distribution of the steep tracks was estimated.

As experiment showed, the number of the charged π-mesons decreases as the angle of emission increases. So an angular distribution of the identified charged π-mesons (Figs. 5 and 6 curve B) was drawn. Multiplying curve B by curve A, and normalizing the new distribution so formed to 100 percent, the angular distribution for the steep tracks in the lab system was arrived at (Figs. 5 and 6, Curve C). Assuming the ratio of proton to $\pi^{\pm}$ mesons in the steep tracks was the same as in the identified tracks, the number of π^{*}-mesons from the steep tracks was found. These steep π^{*}-mesons were then assigned to different angles by means of curve C (Figs. 5 and 6).

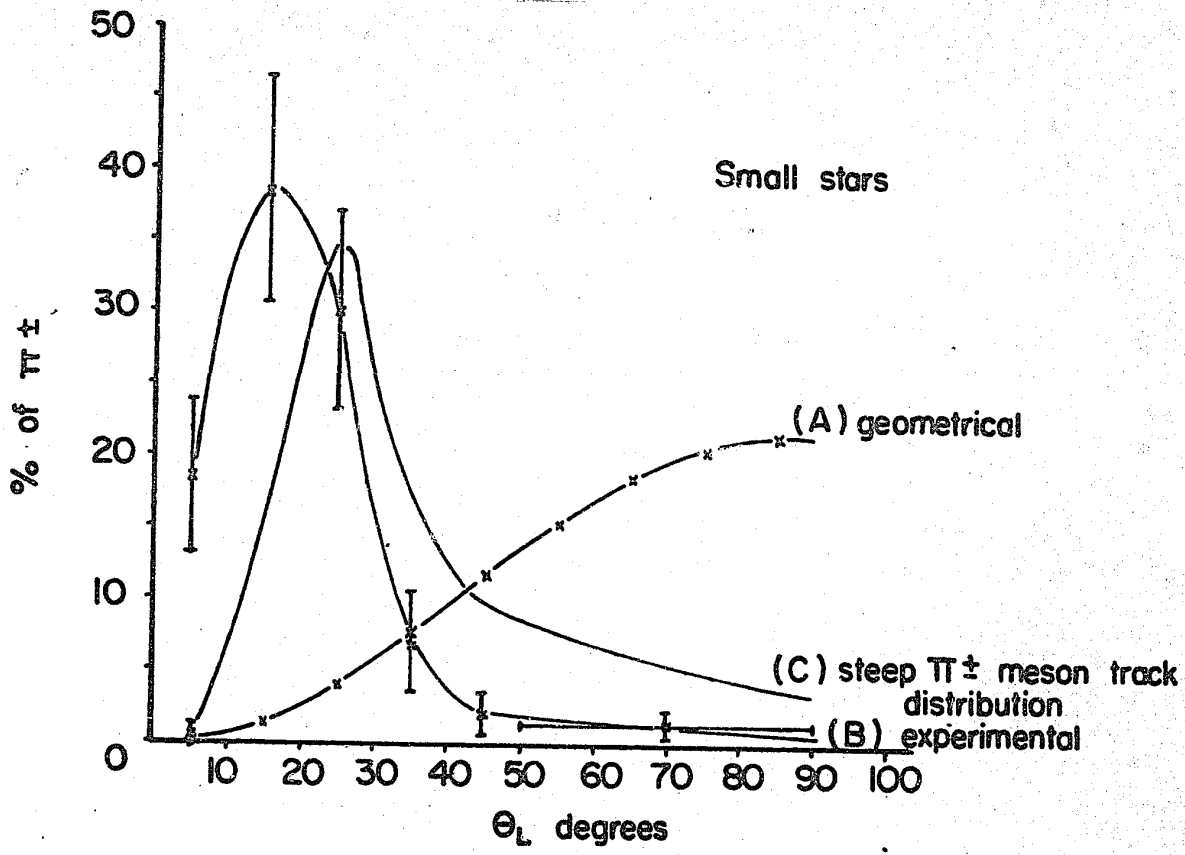

Fig. 5– Correction graphs for steep π ± mesons (all curves normalized to 100 %)

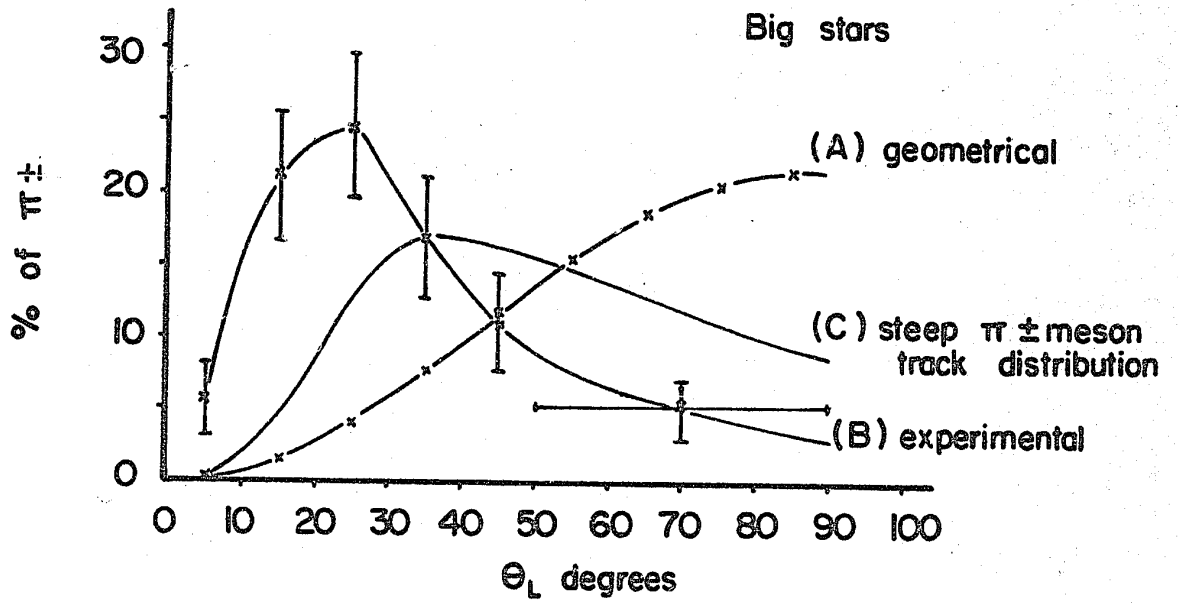

Fig. 6– Correction graphs for steep π ± mesons (all curves normalized to 100 %)

7. EXPERIMENTAL RESULTS

Shower tracks from 68 big stars* and 51 small stars were analysed, the result of which is shown in Table I. In this table, the shower tracks were divided into five groups: proton tracks, $\pi^{\pm}$-meson tracks, steep tracks, high energy tracks and unidentified tracks.

TABLE I

	Small Stars	Big Stars
No. of stars	51	68
No. of protons	28	180
No. of $\pi^{\pm}$-mesons	61	94
No. of steep tracks	40	209
No. of high energy tracks	10	20
No. of unidentified tracks	5	10
Total number of shower tracks	144	513

Assuming that the ratio of protons to $\pi^{\pm}$-mesons in the steep, the high energy and the unidentified tracks was the same as in the identified tracks, the number of $\pi^{\pm}$-mesons from these tracks was calculated. The results are shown in Table II.

*34 big stars were analysed by John Ancsin (thesis, University of Ottawa, 1960). Ten of these stars were remeasured and the result showed good agreement.

TABLE II

	Small Stars	Big Stars
No. of steep $\pi^{\pm}$-mesons	27	72
No. of high energy $\pi^{\pm}$-mesons	7	7
No. of $\pi^{\pm}$-mesons (from unidentified tracks)	3	3
No. of $\pi^{\pm}$-mesons (identified)	61	94
Total number of $\pi^{\pm}$-meson	98	176

8. MESON MULTIPLICITY*

From the results in Table II, the average number of $\pi^{\pm}$-mesons per star is:

$\langle n^{\pm} \rangle = 1.9 \pm .2$ for small stars

and $\langle n^{\pm} \rangle = 2.6 \pm .2$ for big stars

In the calculation of the error for the $\pi^{\pm}$-meson multiplicity, it is assumed that the numbers in the last row of Table II are all $\pi^{\pm}$-mesons. Hence the $\pi^{\pm}$-meson multiplicity produced in heavy nuclei is higher than in light nuclei. This can be explained by considering the energy available in the C. M. system.

9. ENERGY AVAILABLE IN THE C. M. SYSTEM

Suppose the incident proton moves with kinetic energy, E_L, in the lab system and collides with an emulsion nucleus. During the collision,

*Please see appendix.

only part of the nucleus will take part in the interaction for meson production. Let the rest mass energy of this target mass involved be χ. Then the total energy, U_L, of the system in the lab system will be given by

$$U_L = E_L + \mu + \chi \qquad \text{- - - - (9.1)}$$

where μ = rest mass energy of the incident proton.

In the C. M. system, the total energy, U^*, of the system becomes:

$$U^* = \frac{U_L}{\gamma_c} \qquad \text{- - - - (9.2)}$$

where

$$\gamma_c = \left(1 - \beta_c^2\right)^{-\frac{1}{2}} \qquad \text{- - - - (9.3)}$$

and β_c = velocity of the C. M. system relative to the lab system in units of velocity of light, c.

Then equation (9.2) can be written as

$$U^* = U_L \left(1 - \beta_c^2\right)^{\frac{1}{2}} \qquad \text{- - - - - - (9.4)}$$

But

$$\beta_c = \frac{c\,p}{U_L}$$

where p = momentum of the incident proton in the lab system.

Therefore equation (9.4) becomes

$$U^* = U_L\left(1-\frac{c^2p^2}{U_L^2}\right)^{\frac{1}{2}}$$

$$= \left(U_L^2 - c^2p^2\right)^{\frac{1}{2}} \qquad \text{------ (9.5)}$$

But $$\left(E_L+\mu\right)^2 = c^2p^2 + \mu^2$$

or $$c^2p^2 = E_L^2 + 2\mu E_L \qquad \text{---- (9.6)}$$

Substituting the values of U_L and c^2p^2 from (9.1) and (9.6) respectively into (9.5)

$$U^* = \left[\left(E_L+\mu+x\right)^2 - \left(E_L^2+2\mu E_L\right)\right]$$

$$= \left(\mu^2+x^2+2\mu x+2xE_L\right)^{\frac{1}{2}} \qquad \text{--- (9.7)}$$

Hence the energy available in the C. M. system is given by,

$$E^* = U^* - \left(\mu+x\right)$$

or $$E^* = \left(\mu^2+x^2+2\mu x+2xE_L\right)^{1/2} - \left(\mu+x\right) \qquad \text{--- (9.8)}$$

From equation (9.8), it can be seen that this energy increases with x i.e. the target mass involved in the interaction.

On the basis of the tunnel model, the length of the tunnel depends on where the incident proton punches through the nucleus. But on the whole the mean tunnel length with the heavy nuclei should be

greater than that with the light nuclei, since the nuclear diameter is proportional to the cube root of the mass number of the nucleus. This means that the target mass involved in the interaction with the heavy nuclei is greater than that with the light nuclei and hence the energy available in the C. M. system for the production of mesons is higher. This shows that the $\pi^{\pm}$-meson multiplicity should be higher for big stars than for small stars.

10. ANGULAR DISTRIBUTION OF $\pi^{\pm}$-MESONS

In the analysis of the angular distribution of $\pi^{\pm}$-mesons, the Castagnoli[17] and the Duller and Walker[18] F-plot methods are used. Both methods are based on the equation of transformation of angles from the lab system to the C. M. system. This equation can be written as:

$$\tan \theta_L = \frac{1}{\gamma_c} \cdot \frac{\sin \phi}{\frac{\beta_c}{\beta_\pi} + \cos \phi} \qquad \text{- - - -} \quad (10.1)$$

where θ_L = angle of emission of π-meson in the lab system,

ϕ = angle of emission of π-meson in the C. M. system,

β_c = velocity of the centre of mass in the lab system,

β_π = velocity of π-meson in the C. M. system.

In the Castagoli method, the following assumptions are made:

(1) The mesons are produced from nucleon-nucleon collision.

(2) The angular distribution of the mesons is symmetrical with respect to a plane perpendicular to the incident proton and passing through the centre of the emulsion star.

(3) The mesons are independent from one another in the sense that there is no correlation between their angles of emission nor between their energies of emission.

Taking the logarithm on both sides of equation (10.1),

$$\log(\cot\theta_L) = \log\gamma_c - \log\frac{\sin\phi}{\beta_c/\beta_\pi + \cos\phi}$$

For n mesons, the equation can be written as:

$$\frac{1}{n}\sum_{i=1}^{n}\log(\cot\theta_{L_i}) = \log\gamma_c - \frac{1}{n}\sum_{i=1}^{n}\log\frac{\sin\phi_i}{\beta_c/\beta_{\pi_i} + \cos\phi_i} \quad ---(10.2)$$

The term $\log(\cot\theta_L)$ can be found, since θ_L can be measured in the lab. system, while the term $\frac{\sin\phi}{\beta_c/\beta_\pi + \cos\phi}$ depends on the energy and the angle of emission of the meson in the C. M. system. Hence in the "spectrum independent" approximation as suggested by Castagnoli, β_π is put equal to β_c , and we have:

$$\frac{1}{n}\sum_{i=1}^{n}\log\frac{\sin\phi_i}{\beta_c/\beta_{\pi_i} + \cos\phi_i} = \frac{1}{n}\sum_{i=1}^{n}\log\frac{\sin\phi_i}{1+\cos\phi_i}$$

If n is sufficiently large, it can be shown that:

$$\frac{1}{n}\sum_{i=1}^{n}\log\frac{\sin\phi_i}{1+\cos\phi_i} = 0$$

Hence equation (10.2) becomes

$$\log \gamma_c = \frac{1}{n} \sum_{i=1}^{n} \log(\cot \theta_{L_i}) \quad \text{------- (10.3)}$$

By Laplace Theorem, the distribution of $\log(\cot\theta_L)$ can be shown to be a Gaussian distribution. The mean of this distribution is equal to $\log \gamma_c$. Hence by the Castagnoli method, $\log \gamma_c$ can be found. But from equations (9.1), (9.2) and (9.7), γ_c can be written as:

$$\gamma_c = \frac{E_L + \mu + x}{(\mu^2 + x^2 + 2\mu x + 2x E_L)^{1/2}} \quad \text{--- (10.4)}$$

Therefore, for a given target mass, x, involved, the corresponding $\log \gamma_c$ can be calculated. Thus the target mass can be found from the distribution of $\log(\cot\theta_L)$.

In the F-plot method, the assumption that $\beta_\pi = \beta_c$ is also used. Therefore the equation transforming angles from the lab system to the C. M. system can be written as:

$$\tan\theta_L = \frac{1}{\gamma_c} \cdot \frac{\sin\phi}{1 + \cos\phi}$$

or

$$\tan\theta_L = \frac{1}{\gamma_c} \tan\frac{\phi}{2}$$

Squaring both sides of the equation, we get

$$\tan^2\theta_L = \frac{1}{\gamma_c^2} \cdot \frac{\sin^2 \phi/2}{1 - \sin^2 \phi/2} \qquad \text{- - - - (10.5)}$$

Assuming spherical symmetry of the angular distribution of π-mesons in the C. M. system, the number of π-mesons passing through a spherical surface of radius r and with the centre of the emulsion star as the centre, will be directly proportional to the surface area. The spherical surface subtending a semi-angle ϕ at the centre is given by:

$$\begin{aligned} S &= 2\pi r^2 \int_0^{\phi} \sin\phi \, d\phi \\ &= 2\pi r^2 (1 - \cos\phi) \\ &= 4\pi r^2 \sin^2 \phi/2 \end{aligned}$$

Hence the fraction F of the number of the π-mesons emitted within the angle ϕ is given by:

$$F = \frac{S}{4\pi r^2}$$

$$\text{i.e.} \qquad F = \sin^2 \frac{\phi}{2}$$

substituting into (10.5), we get

$$\tan^2\theta_L = \frac{1}{\gamma_c^2} \cdot \frac{F}{1-F} \qquad \text{- - - - (10.6)}$$

Hence if a graph of $\log \frac{F}{1-F}$ against $\log(\tan\theta_L)$ is drawn, the slope of the graph should be equal to 2 for isotropic angular distribution for π-mesons in the C. M. system.

The $\log(\cot\theta_L)$ distribution of $\pi^{\pm}$-mesons for small and big stars is shown in Figures 7 and 8, respectively. The arrows show the different expected values of $\log \gamma_c$ as calculated from equation (10.4) for different target masses involved. The solid line histogram represents the total* distribution which includes the identified, the steep and the high energy $\pi^{\pm}$-mesons, while the shaded area represents the distribution for the identified $\pi^{\pm}$-mesons above. The analysis of results shows the mean value of the total distribution as:

$$\langle \log(\cot\theta_L) \rangle = .42 \quad \text{for small stars}$$

and $$\langle \log(\cot\theta_L) \rangle = .12 \quad \text{for big stars}$$

*The three $\pi^{\pm}$-mesons from the unidentified tracks (Table II) in both small and big stars were neglected, since it was impossible to assign any angle to them.

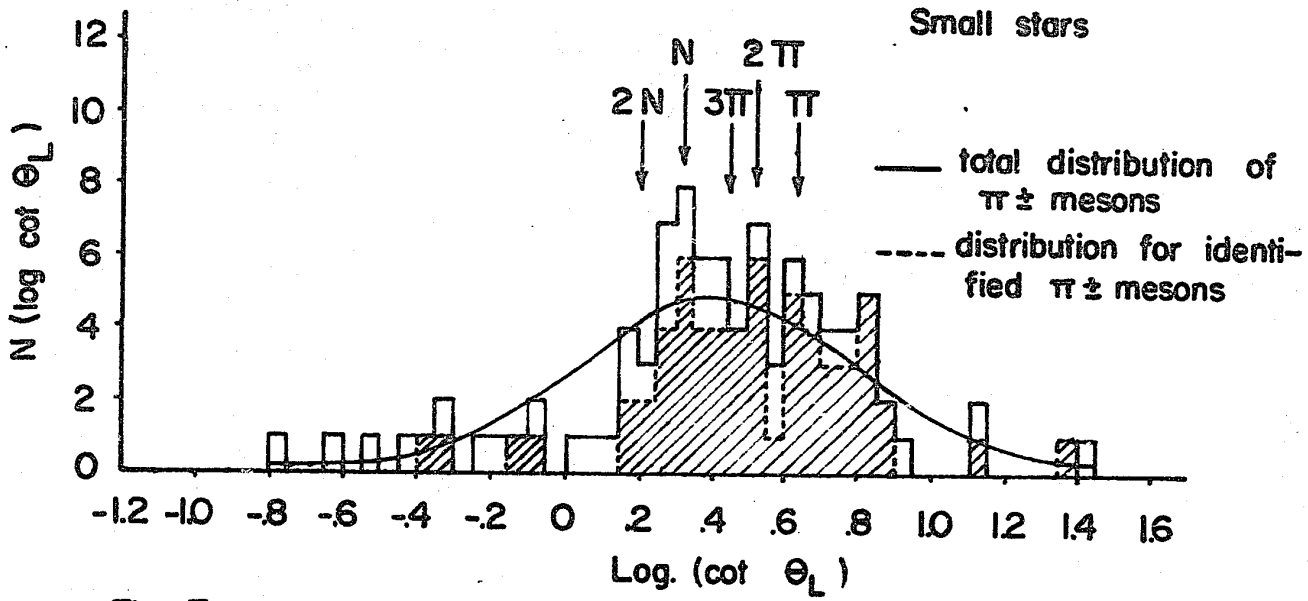

Fig. 7 - π ± meson distribution of log (cot θ_L)

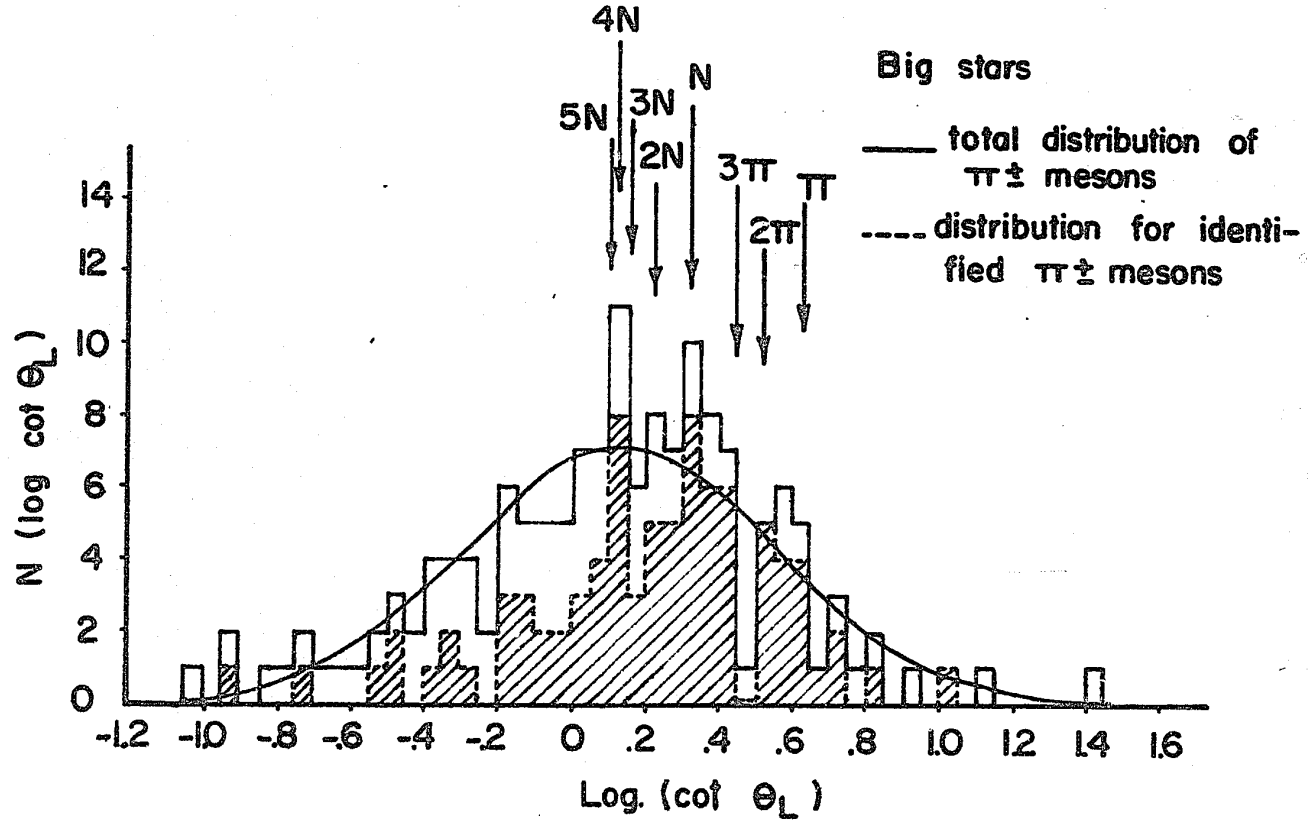

Fig. 8- π ± meson distribution of log (cot θ_L)

and the standard deviation is:

$$\sigma = .39 \text{ for small stars}$$

$$\sigma = .42 \text{ for big stars.}$$

Using these values a gaussian curve which is also shown in the diagram, is fitted to the total distribution and the χ^2-test shows an agreement, since the probability, P, is .7 and .8 for small and big stars respectively. For isotropic angular distribution in the C. M. system, the standard deviation of the gaussian distribution is .36. Therefore the angular distribution for both small and big stars does not show spherical symmetry in the C. M. system.

The above mean value for small stars shows that 0.5 nucleon mass was involved in the interaction, while for big stars, 4 nucleon masses were involved. Since the average target mass in small stars is less than one nucleon mass, this seems to indicate that the incident proton may interact with the meson field of the target nucleon and the π-meson so produced is pushed forward. Now let us examine the distribution more carefully. In small stars, there are peaks round the regions of $\log(\cot\theta_L)$ corresponding to target masses of one nucleon mass, two π-meson mass and one π-meson mass, while in big stars, the peaks correspond to target masses of three, four or five nucleon masses, one nucleon mass and around two or one π-meson masses. (The last one is not so distinct).

In order to show this effect more distinctly, the method proposed by Friedländer[7] was used. For each star consider the arithmetic mean, ξ, of the $\pi^{\pm}$-meson showers in the star.

$$\xi = \frac{1}{n} \sum_{i=1}^{n} \log(\cot\theta_{L_i})$$

The number of shower particles is 2.8 and 7.6 for small and big stars; including the neutral particles assumption (3) in the Castagnoli's method may still be justified without violating laws of conservation of energy and momentum. Therefore we are justified in finding the value of ξ for each individual star. If a single type of target mass is involved, the ξ-distribution for all stars should assume a gaussian distribution as the $\log(\cot\theta_L)$ distribution does, with the mean corresponding to a certain target mass involved. As it was impossible to tell whether the steep tracks, the high energy tracks, and the unidentified tracks were protons or $\pi^{\pm}$-mesons, only the identified $\pi^{\pm}$-meson tracks were used to calculate the value of ξ. The ξ-distribution for small stars and big stars is shown in Figs. 9 and 10 respectively. In the small stars, there is one pack between one nucleon mass and three π-meson mass, one at 2 π-meson mass and another beyond one π-meson mass. The peak beyond one π-meson mass seems to indicate that the incident proton interacts with the π-meson field of the target nucleon and the π-meson so produced is pushed out in a forward direction at a small angle with respect to the incident proton. If this is the case, this accounts for the peak beyond the one π-meson mass, and the $\log(\cot\theta_L)$ distribution for such π-meson is no more gaussian. In the ξ-distribution for big stars, one peak exists around, three, four or five nucleon masses, one between one nucleon mass and 3 π-meson mass and another at one π-meson mass. In order to separate these peaks, arbitrary ranges of ξ are chosen. From the figures it seems reasonable to separate the small stars into two groups: one with $\xi > .4$ and another with $\xi < .4$. In the big stars, the stars are divided into

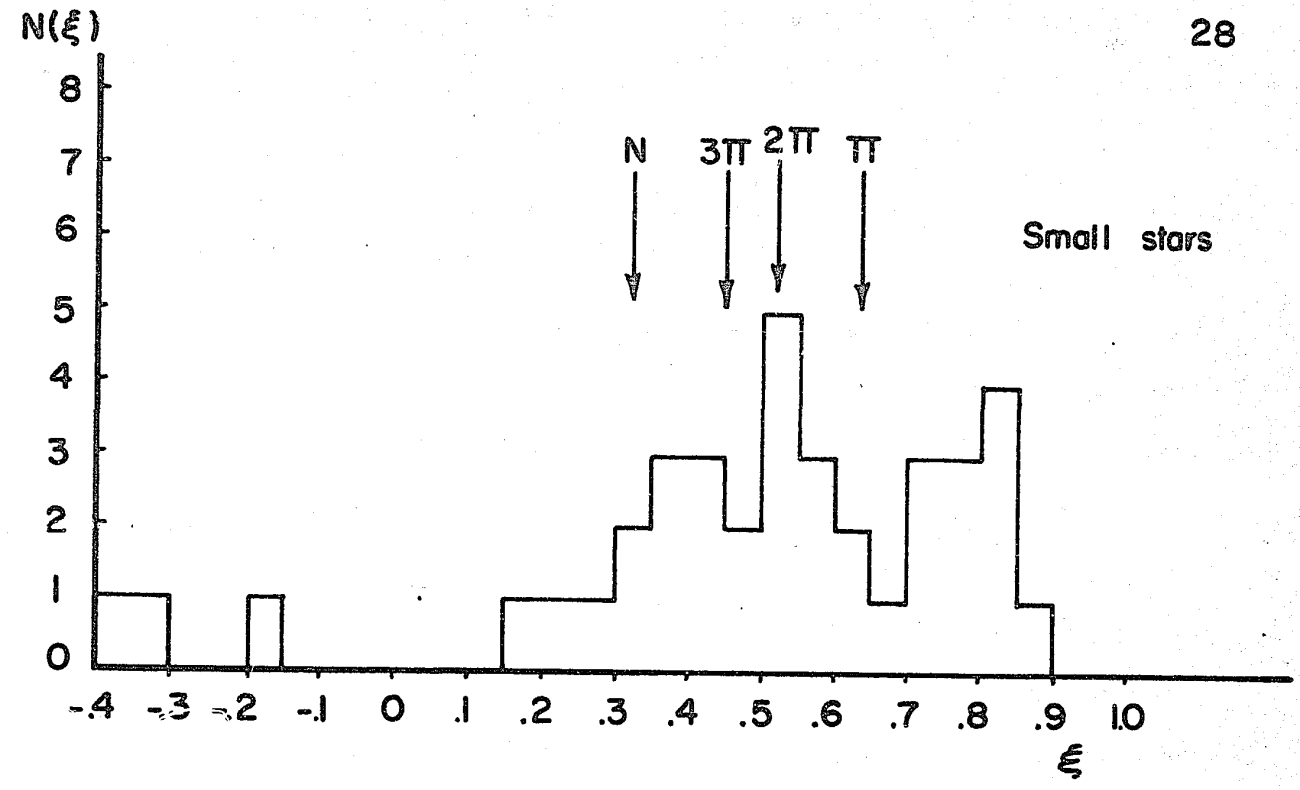

Fig. 9- Distribution of ξ

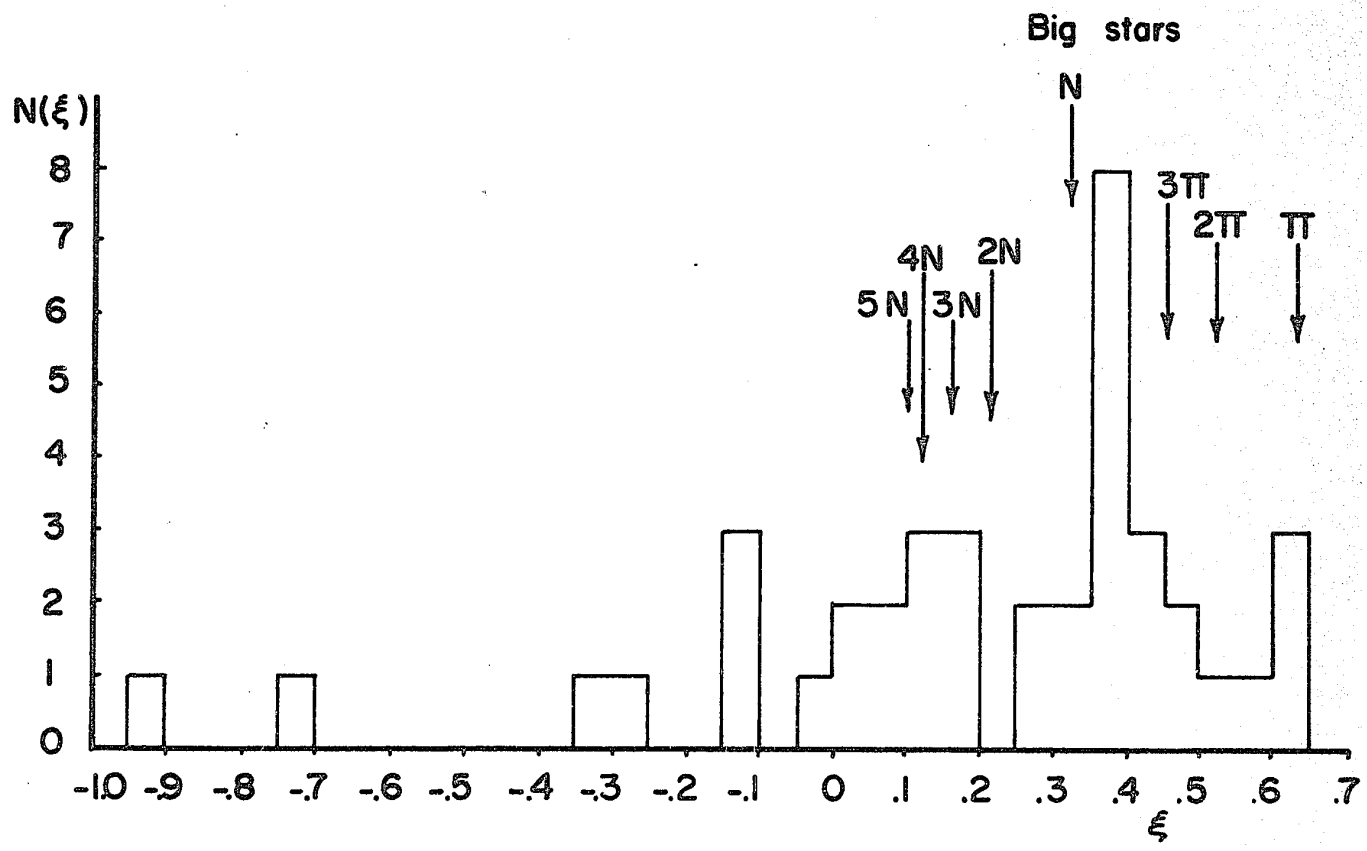

Fig. 10- Distribution of ξ

three groups: one with $\xi < .2$, one with $.2 < \xi < .4$, and the remaining one with $\xi > .4$. The $\log(\cot\theta_L)$ distributions for all these groups are shown in Figs. 11, 12, 13, 14, and 15. With small stars, the group with $\xi > .4$ (Fig. 11) shows peaks at 3 π-meson, 2 π-meson and 1 π-meson masses and the peak beyond one π-meson mass remains. The last peak again seems to indicate that the incident proton interacts with the meson field of the target nucleon. In the other group where $\xi < .4$ (Fig. 12) the distribution shows a distinct peak at one nucleon mass. In the big stars, the group of $\xi < .2$ (Fig. 13) shows a distinct peak at three, four or five nucleon masses, the group of $.2 < \xi < .4$ (Fig. 14) shows a peak at one nucleon mass and the group of $\xi > .4$ (Fig. 15) shows peaks at three π-meson, two π-meson and one π-meson. Hence using this method, the different target masses involved in the interaction separate.

From Figs. 11 and 15, it can be seen that the interaction between the proton and the meson field of the target nucleon in much more prominent with small stars than the big stars. The reason is that in such an interaction, it is very likely that an edge-on collision must take place and such a collision may not be able to produce eight or more black tracks even if the target nucleus belongs to the heavy group. Bonsignori and Selleri[19] have pointed out that this peripheral interaction is important in nucleon-nucleon interaction. The mesons produced this way can be explained by the isobaric nucleon model[20]. In this model, one of the two nucleons interacts with the meson field of the other nucleon and this nucleon forms an isobar with the π-meson. Then this isobar decays and a π-meson is emitted. Sometimes both nucleons are excited to the isobaric state and as a result two π-mesons are produced.

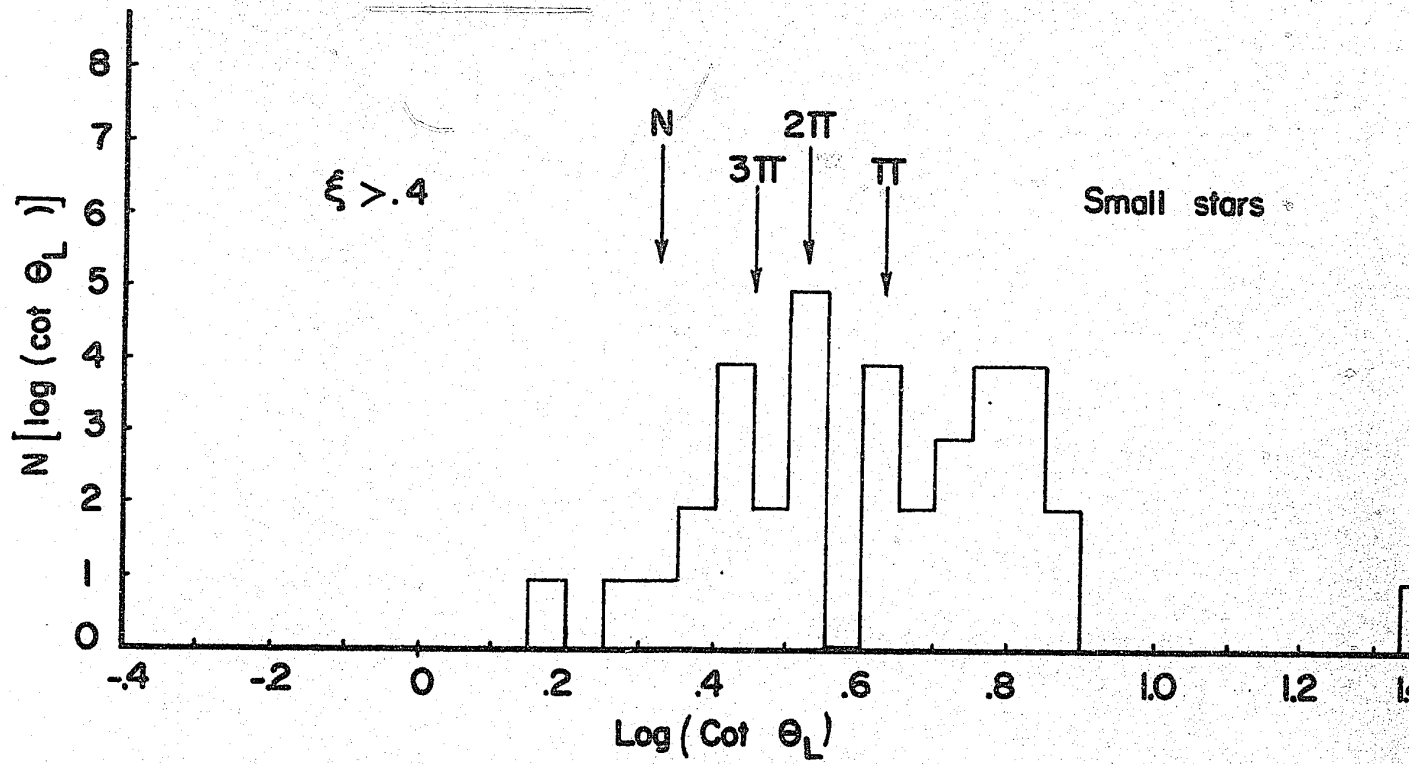

Fig. 11- $\pi^{\pm}$ meson distribution of log (cot θ_L) for $\xi > .4$

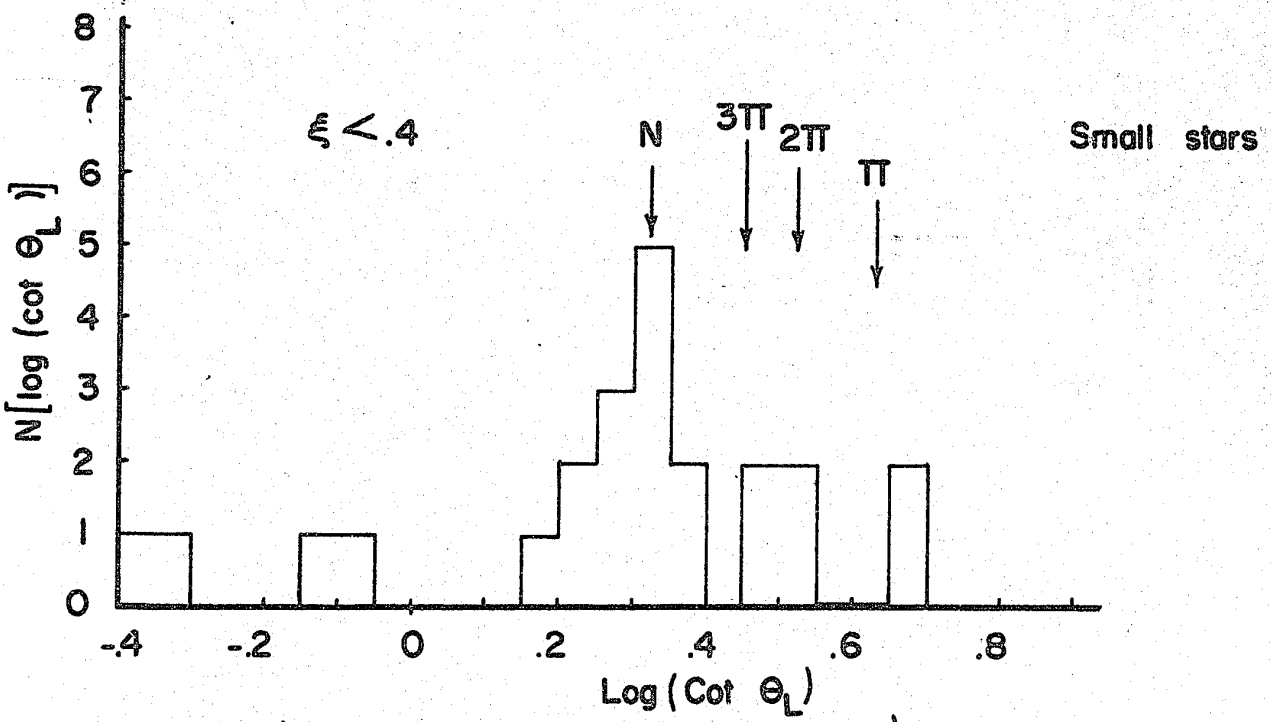

Fig. 12- $\pi^{\pm}$ meson distribution of log (cot θ_L) for $\xi < .4$

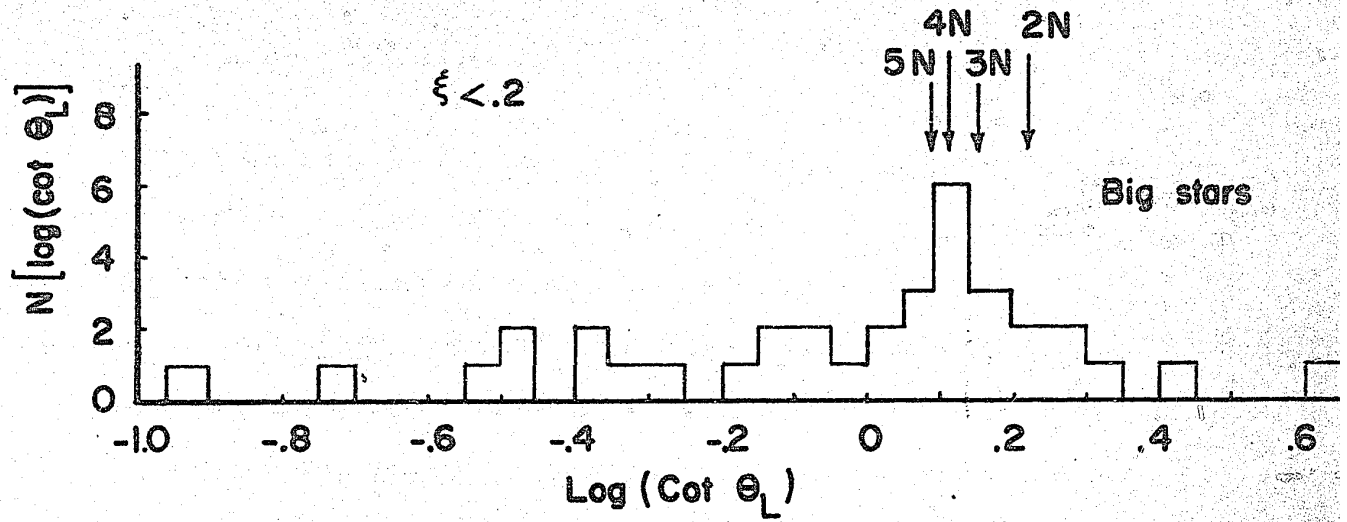

Fig. 13- $\pi^{\pm}$ meson distribution of log (cot θ_L) for $\xi < .2$

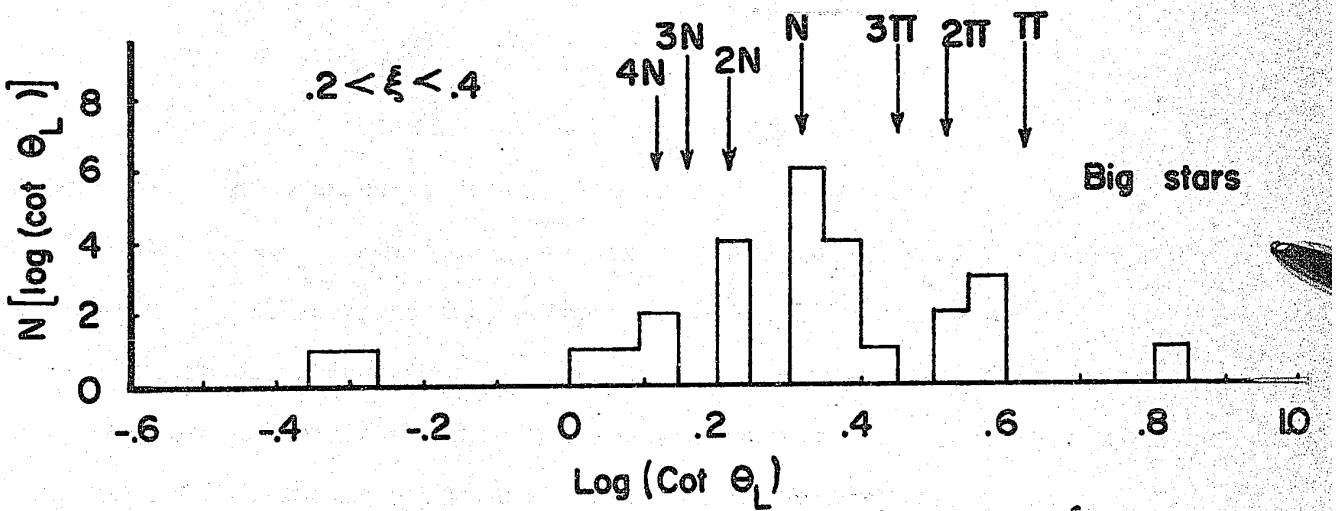

Fig. 14- $\pi^{\pm}$ meson distribution of log (cot θ_L) for $.2 < \xi < .4$

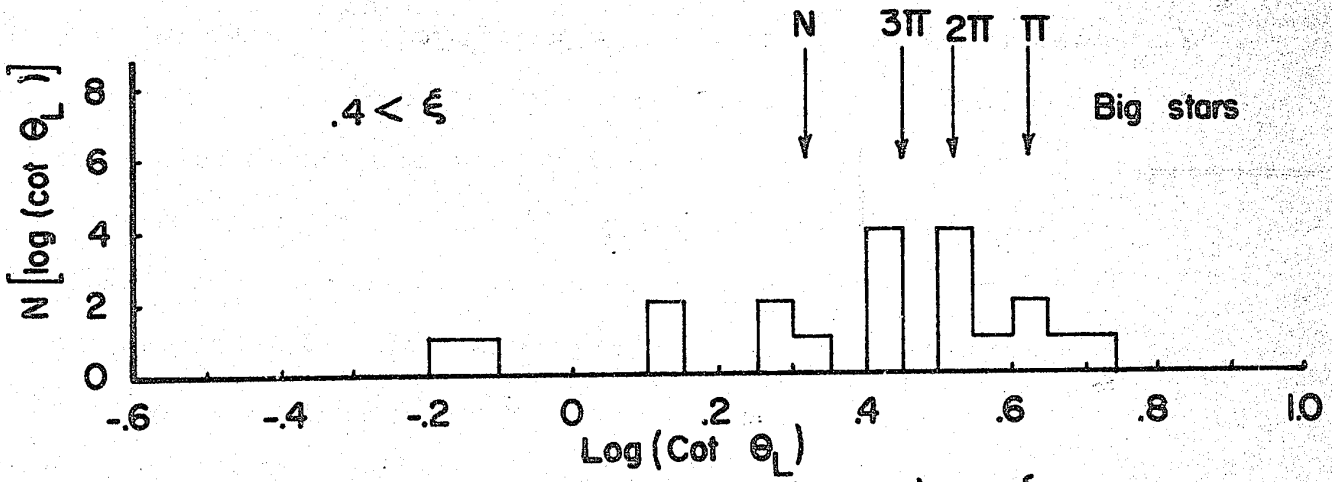

Fig. 15- $\pi^{\pm}$ meson distribution of log (cot θ_L) for $\xi > .4$

The production of π-meson from proton-proton collision through the formation of an isobaric state has recently been investigated by Barnes et al[21] and Melissines et al[22] at 970 Mev and 2.9 Bev respectively. The former used a hydrogen bubble chamber while the latter used a liquid hydrogen target and detected the π-mesons produced at 0°, 17° and 32° with respect to the direction of the incident proton. The three chief interactions are:

$$p + p \rightarrow p + p \qquad \text{- - - - - - - - - (1)}$$

$$p + p \rightarrow p + n + \pi^{+} \qquad \text{- - - - - - - - - (2)}$$

and $$p + p \rightarrow p + p + \pi^{o} \qquad \text{- - - - - - - - - (3)}$$

and some other interactions involving the production of more than one π-meson. Barnes et al showed in their experimental result that the cross sections for the above three interactions as 24.4 ± 1.0, 18.4 ± 0.8 and $3.8 \pm .4$ millibarns respectively. Hence it can be seen that at this proton energy, the production of π-meson is chiefly via interaction (2). In such an interaction the incident proton interacts with the π^{+}-meson in an isobaric state of isotopic spin 3/2 and the neutron acts as a spectactor. Other experimenters[23,24] investigated the same problem with π-meson proton collision in hydrogen bubble chambers and also showed that π-meson was produced via the formation of an isobaric state.

The angular distribution of the identified $\pi^{\pm}$-meson is also studied with the F-plot method. Such a plot for both small and big stars is shown in Figs. 16 and 17, respectively. The straight lines are fitted by the method of least squares. The slopes for small and big stars are found to be 2.4 and 2.1 respectively. This shows that there may be a deviation from isotropy in the C. M. system in the small stars, while in

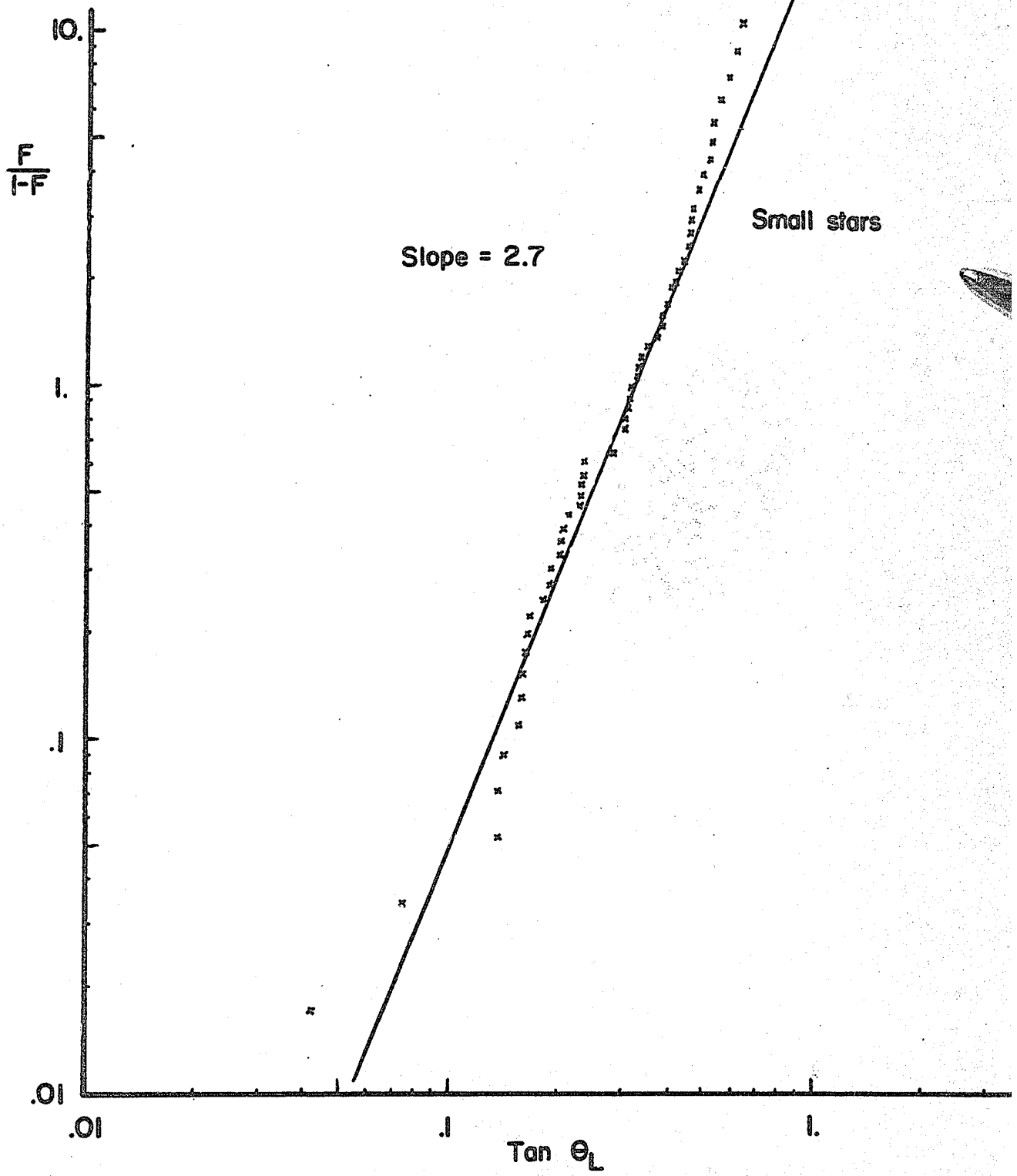

Fig. 16- F-plot of the angular distribution of TT± mesons

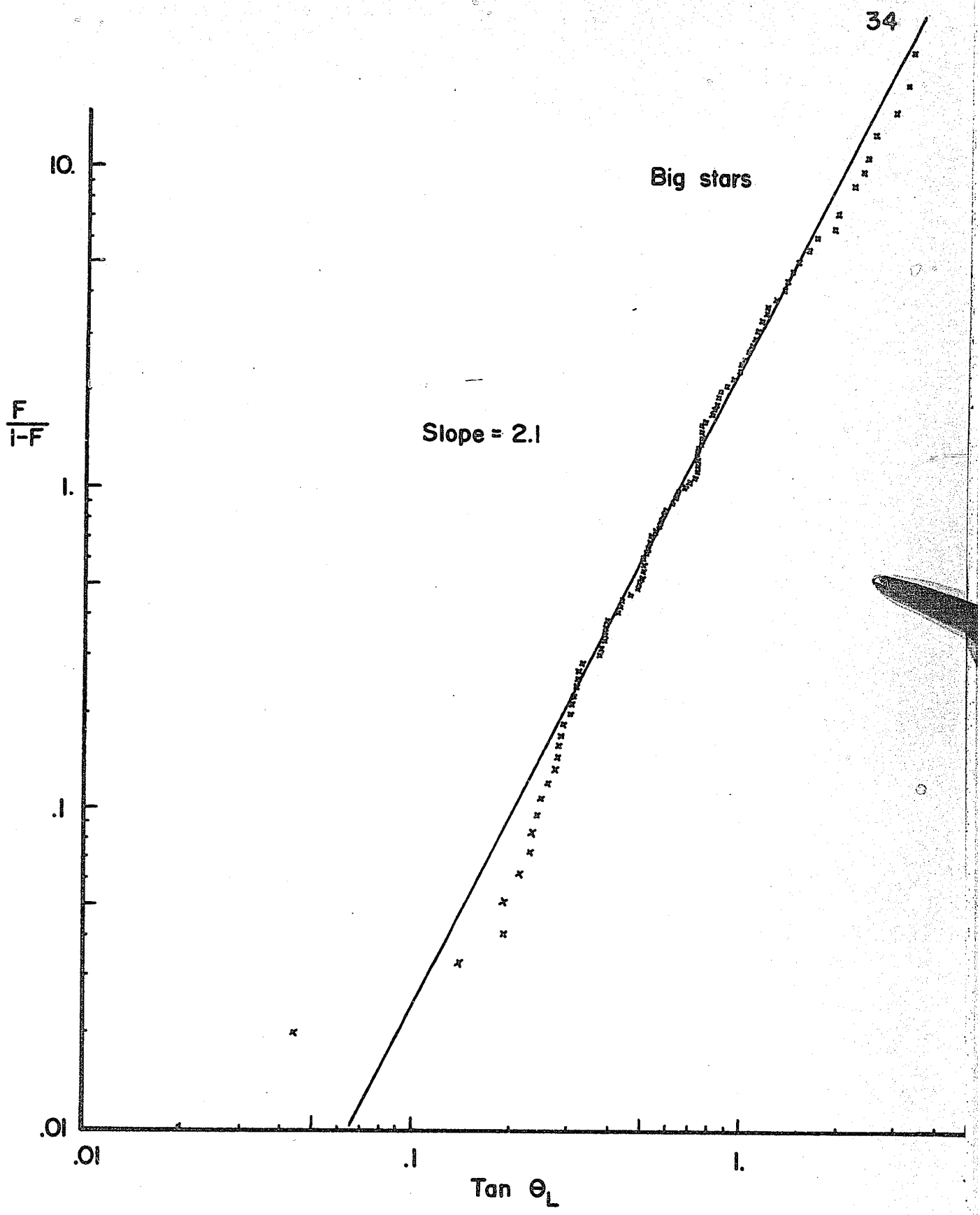

Fig. 17- F-plot of the angular distribution of $\pi^{\pm}$ mesons

Small stars

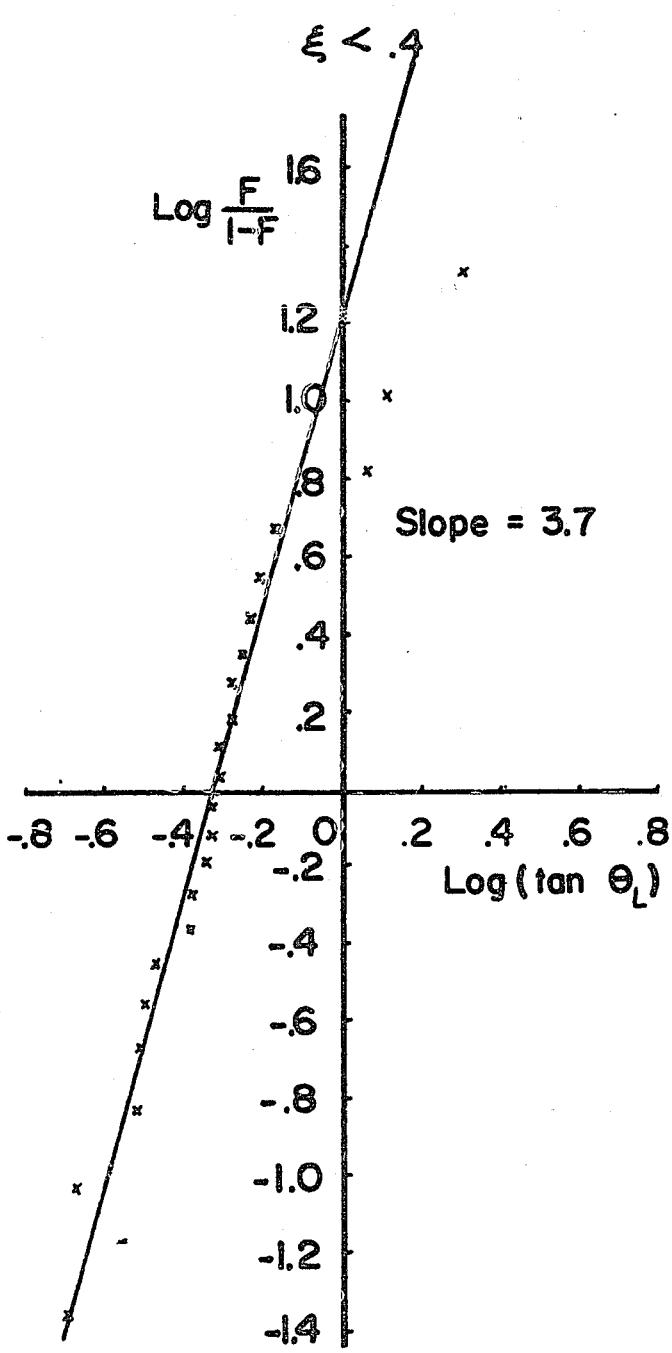

Fig. 18 - F-plot of π± mesons for ξ < .4

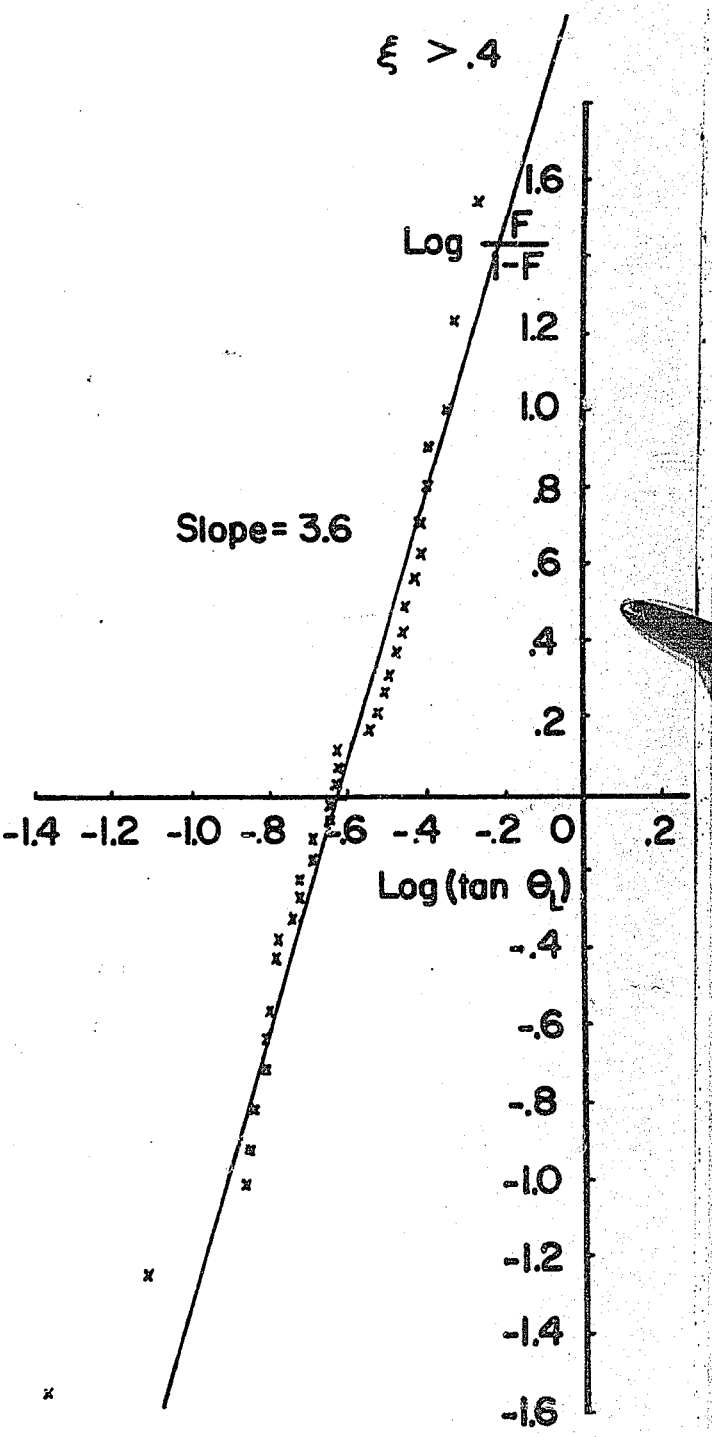

Fig. 19 - F-plot of π± mesons for ξ > .4

Big stars

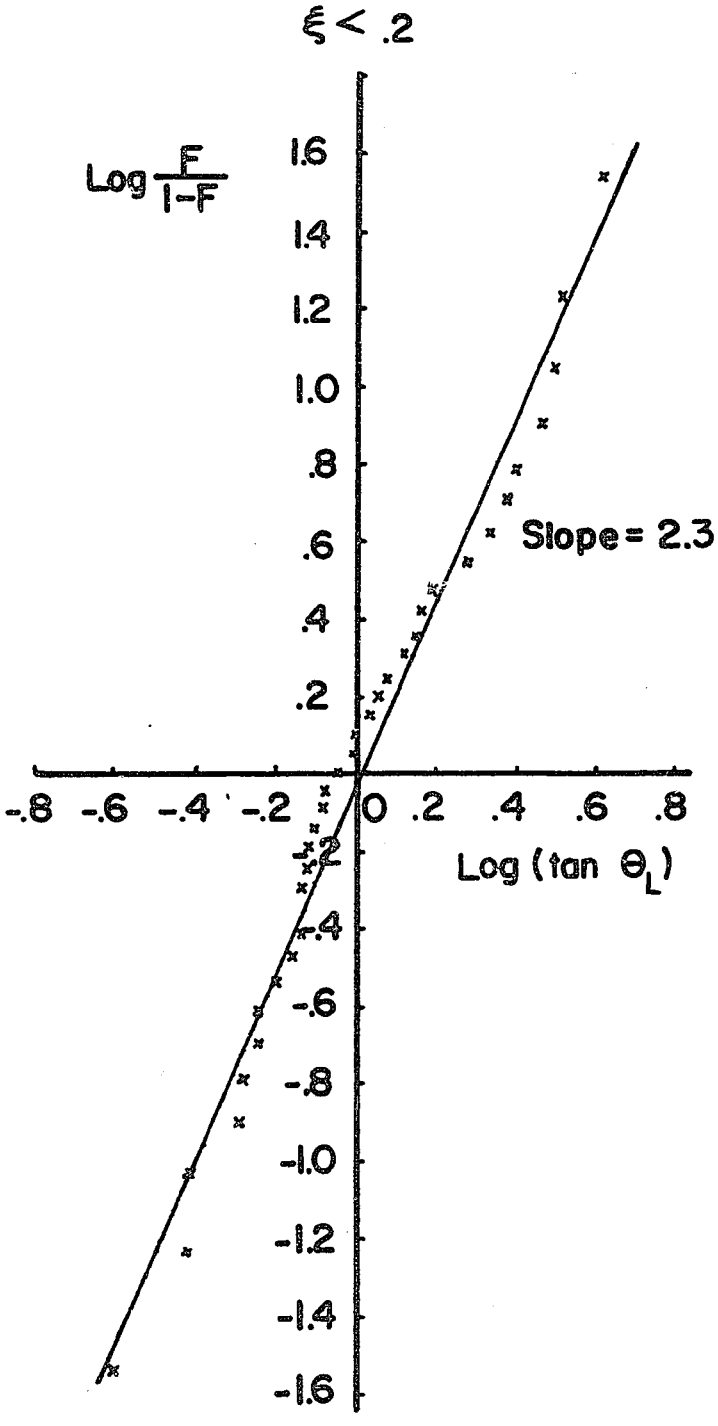

Fig. 20 - F-plot of $\pi^{\pm}$ mesons for $\xi < .2$

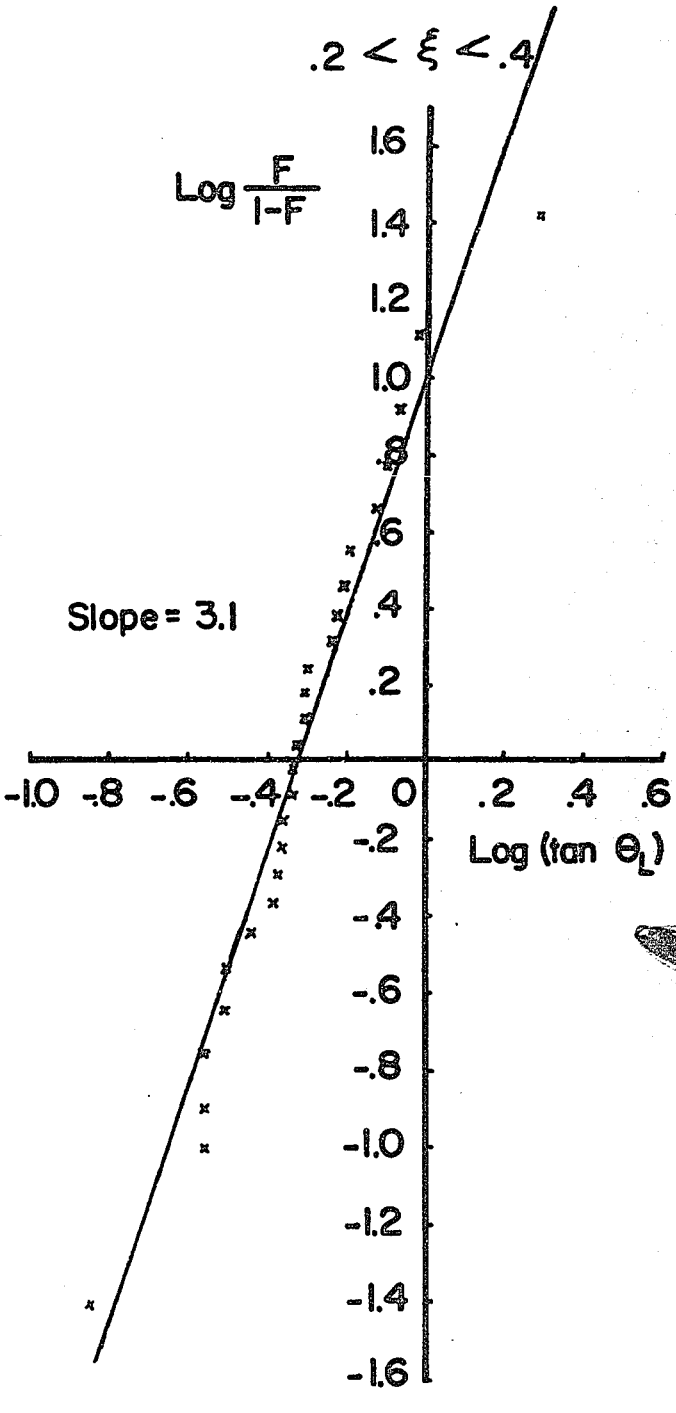

Fig. 21 - F-plot of $\pi^{\pm}$ mesons for $.2 < \xi < .4$

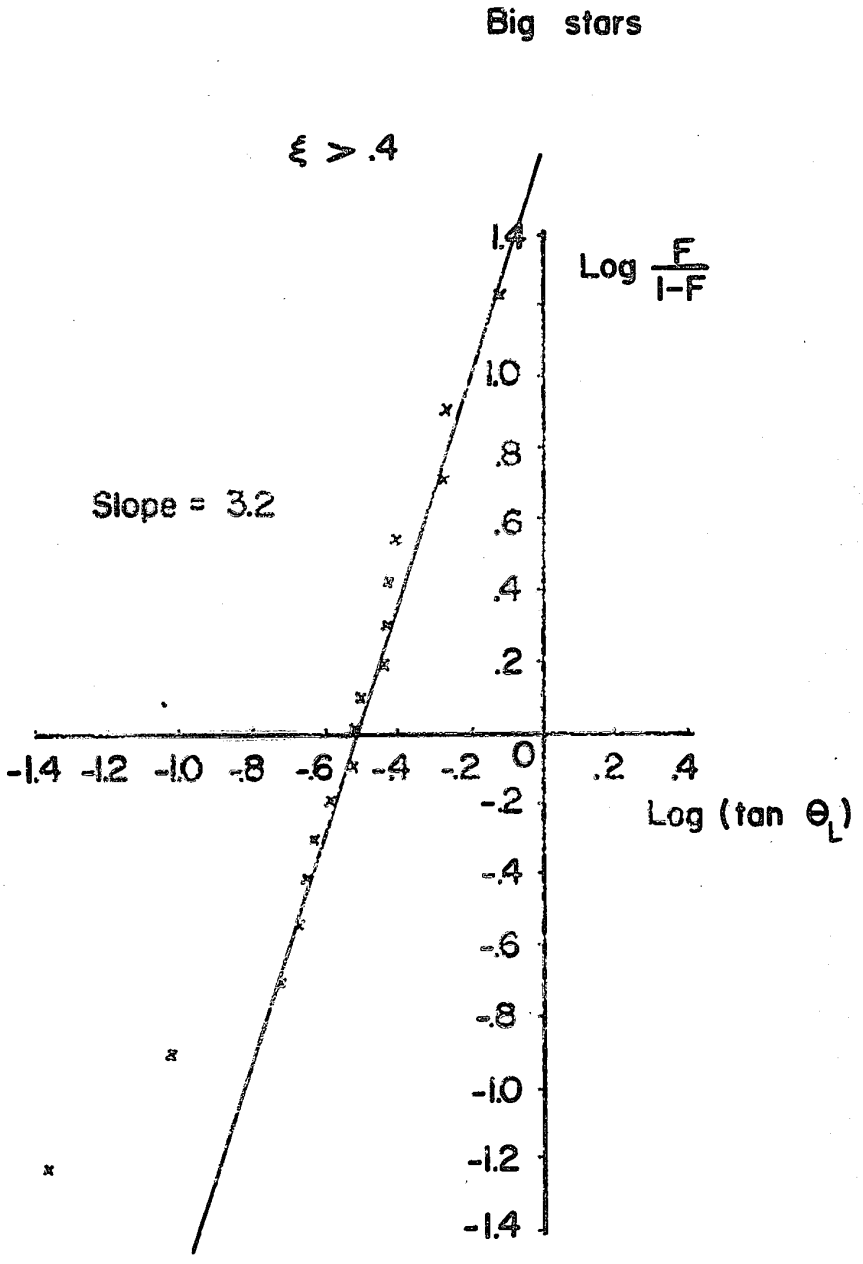

Fig. 22-F-plot of $\pi^{\pm}$ mesons for $\xi > .4$

big stars the angular distribution may be isotropic in the C. M. system. In order to study the angular distribution of the $\pi^{\pm}$-meson for different target masses involved, the same method as used in the $\log(\cot\theta_L)$ distribution, separating stars into different groups is used again.

The small stars are divided into two groups: one with $\xi > .4$ and one with $\xi < .4$ and the big stars are divided into three groups: one with $\xi < .2$, one with $.2 < \xi < .4$ and the remaining one with $\xi > .4$. The F-plots of these groups are shown in Figs. 18, 19, 20, 21 and 22. All these straight lines are again fitted by the method of least squares, and all except the one with $\xi < .2$ (Fig. 20) in big stars, show a slope much bigger than 2, which is the slope for isotropic angular distribution in the C. M. system. Therefore, the angular distribution of the $\pi^{\pm}$-meson shows anisotropy in the C. M. system for the cases where the target masses involved are one nucleon mass and the meson field of the target nucleon. This shows an agreement with the work on the inelastic collision between 6.2 Bev. protons and nucleons (hydrogen atoms and peripheral nucleons in the emulsion) by Kalbach et al[6] and Daniel et al[9], in which they showed that the angular distribution of the $\pi^{\pm}$-mesons showed forward and backward peaking in the C. M. system. For the group in big stars with $\xi < .2$, which corresponds to three, four or five nucleon target masses, the angular distribution in the C. M. system may be isotropic, as the slope of the graph is 2.3.

11. TRANSVERSE MOMENTUM

Rosental' and Milekhin were the first to draw attention to connection between the angle and the energy of emission of secondary particles in high energy nuclear interactions. In their hydrodynamical

model[25] for multiple particles production, the secondary particles are assumed to be produced as result of particles in thermal motion at an evaporation temperature of $\mu c^2/k$, where μc^2 is the rest mass energy of π-meson and k is the Boltzmann constant. In such a process, the transverse momentum (the component of the momentum perpendicular to the direction of the incident particle) of the secondary particles vary only slightly over a relatively large range of the angles of emission. Therefore, the distribution of the transverse momenta is a gaussian distribution with a mean at 1 μc. For convenience sake [26], instead of plotting a distribution for the transverse momentum, p, $\log(\frac{p_t}{\mu c})$ is plotted.

The transverse momenta distribution for small and big stars is shown in Figs. 23 and 24, respectively. The solid line histogram shows the total distribution for identified $\pi^{\pm}$-mesons and the curve is the gaussian curve fitted to the experimental data, and the χ^2-test shows an agreement, since the probability, P, is .5 and .3 for small and big stars respectively. The mean values of the transverse momentum distributions are 0.59 μc and 0.84 μc for small and big stars respectively. Also such a distribution for small and big stars, in which $\xi > .4$, is shown as shaded area in the same figures. As seen from the figures, both distributions show a mean less than that for the total distribution. Thus taking off those $\pi^{\pm}$-mesons produced in the peripheral interaction, the mean value for the transverse momentum distribution will shift towards the value of 1 μc, as predicted by the theory.

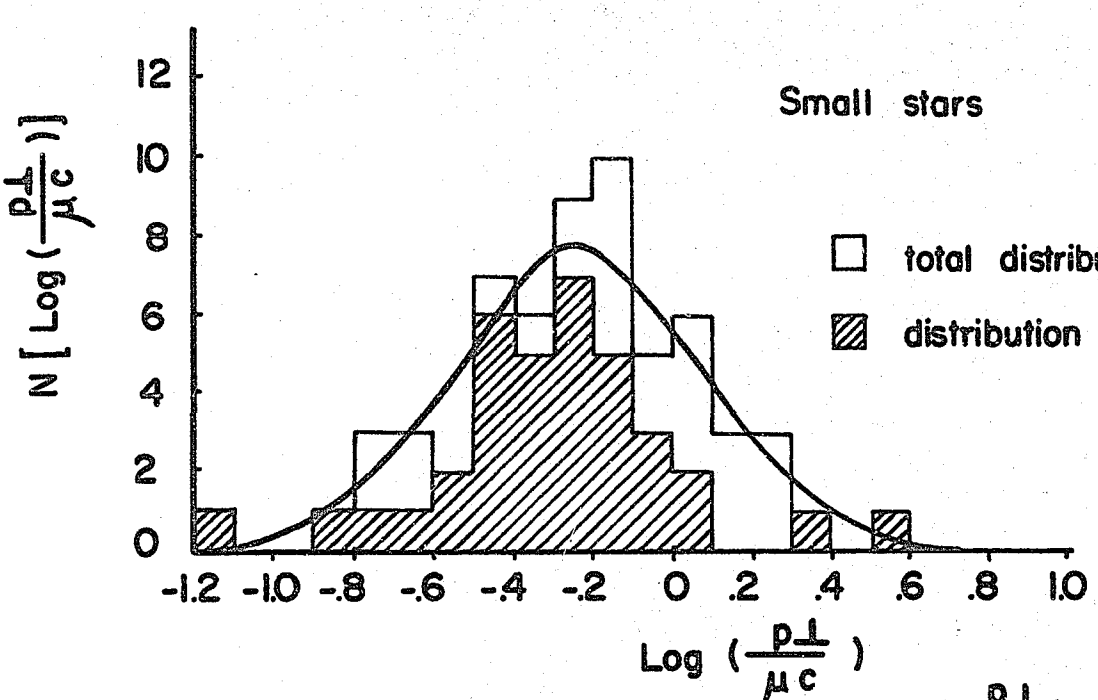

Fig. 23-TT± meson distribution of log $\left(\frac{p_\perp}{\mu c}\right)$

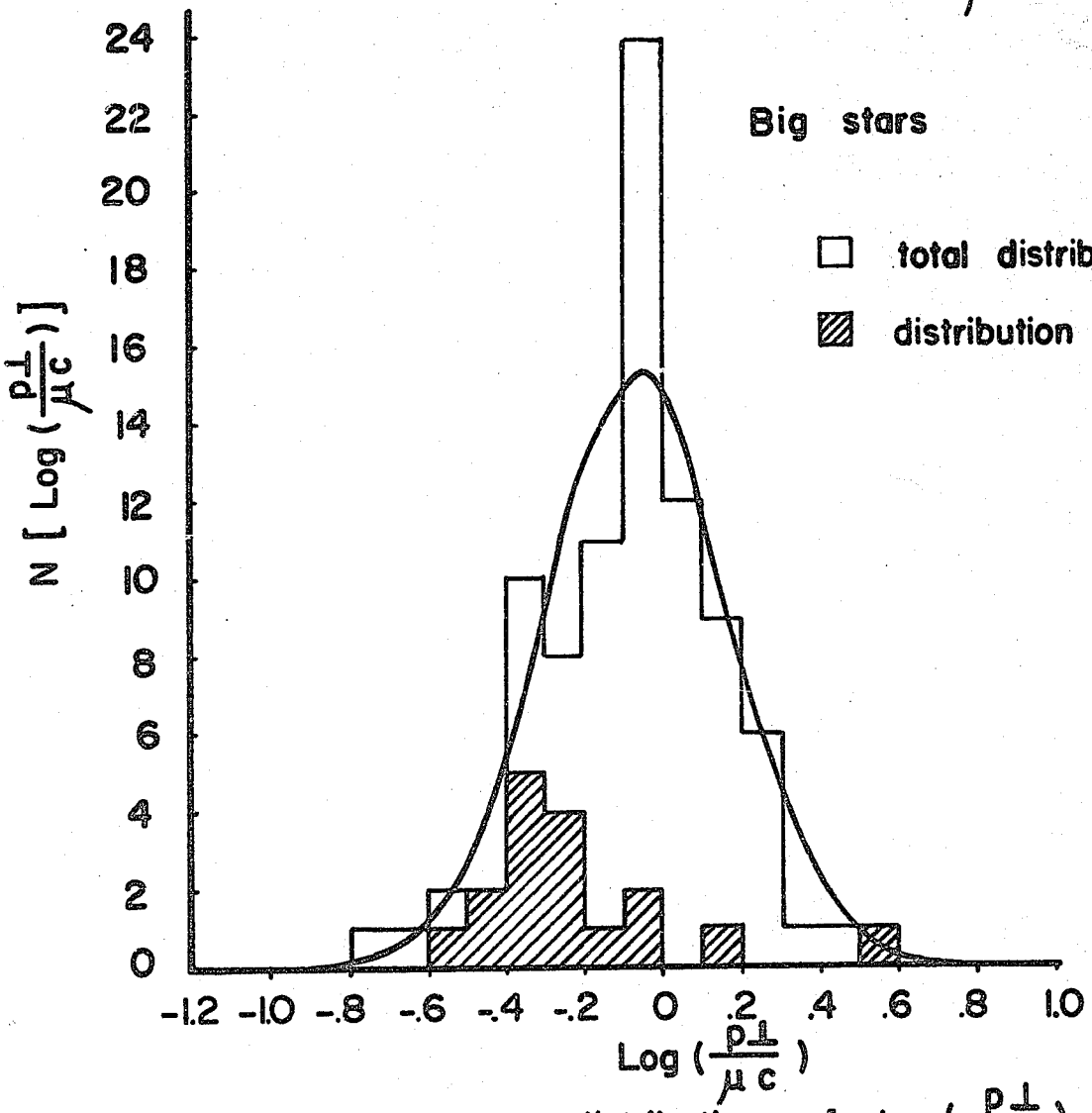

Fig. 24-TT± meson distribution of log $\left(\frac{p_\perp}{\mu c}\right)$

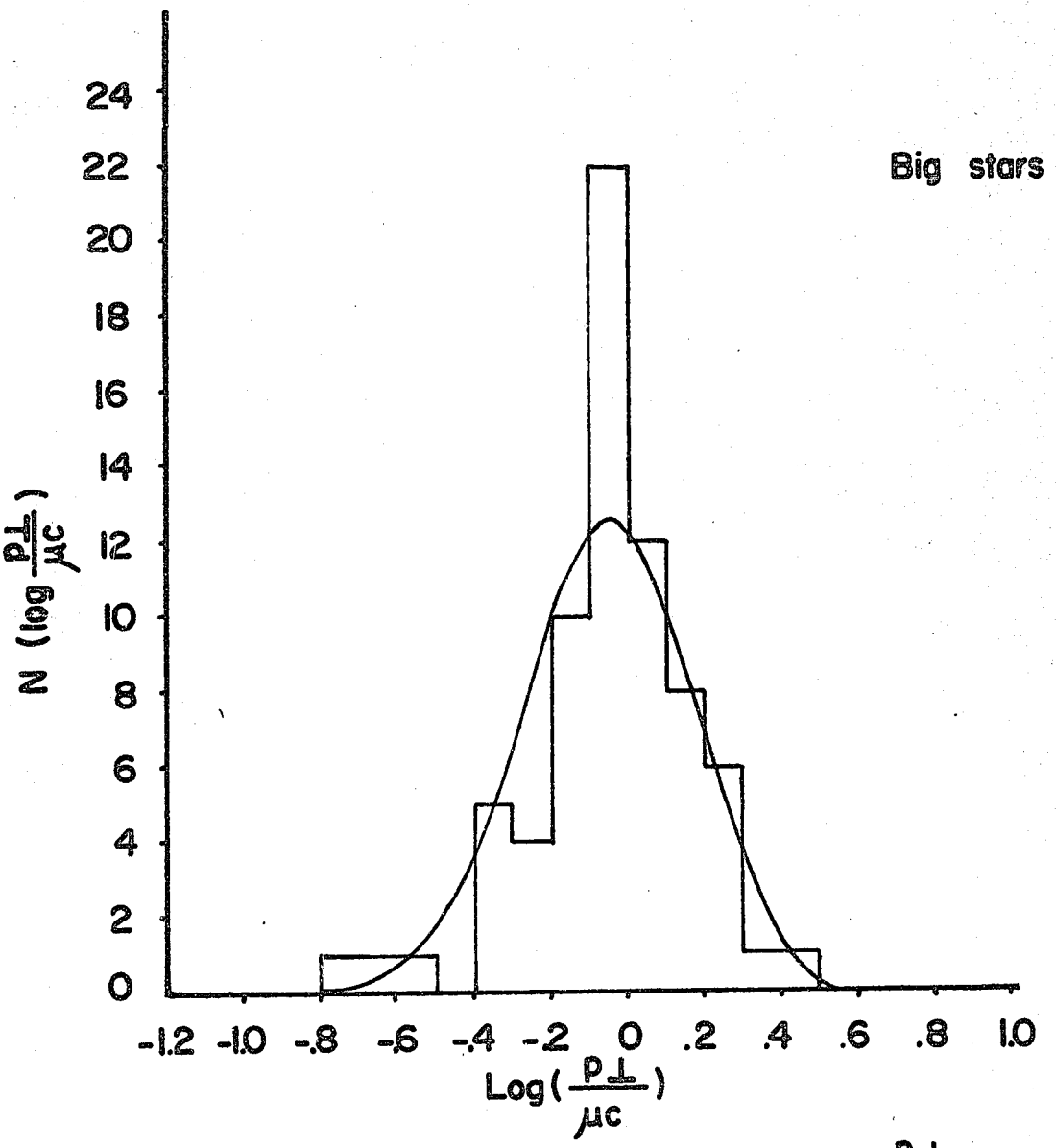

Fig. 25– $\pi^{\pm}$ meson distribution of log. ($\frac{p_\perp}{\mu c}$) for $\xi < .4$

In the small stars, many of the events are due to the interaction of the incident proton and the meson field of the peripheral nucleons so after taking off these events in the $\log(\frac{p_\perp}{\mu c})$ distribution, the statistics would be too poor to show the $\log(\frac{p_\perp}{\mu c})$ distribution for the case where one target nucleon mass is involved. But in the big stars, these events are removed and the remaining distribution is shown in Fig. 25. The mean value for such a distribution is .90 μc. The curve is again a gaussian curve fitted to the experiment data. The agreement between the curve and the experimental data is not so good as before, since the probability, P, from the χ^2-test is .12. Thus it can be seen that the mean value of the transverse momentum distribution in the cases where the target mass is at least one nucleon mass, is close to the theoretical value.

12. ENERGY SPECTRUM OF $\pi^{\pm}$-MESONS

Finally, the energy spectrum for the identified $\pi^{\pm}$-mesons is studied. The energy spectrum for big and small stars is shown in Figs. 26 and 27, respectively. In big stars, the spectrum shows a maximum at the interval 100-150 Mev and then drops off quite rapidly with increasing energy. For small stars, the maximum is at the interval 50-100 Mev and the spectrum drops off less rapidly with increasing energy. This indicates that there is a higher proportion of higher energy $\pi^{\pm}$-mesons produced in small stars, as the $\pi^{\pm}$-mesons produced from peripheral interaction may have higher energy as compared with those due to a larger target mass interaction.

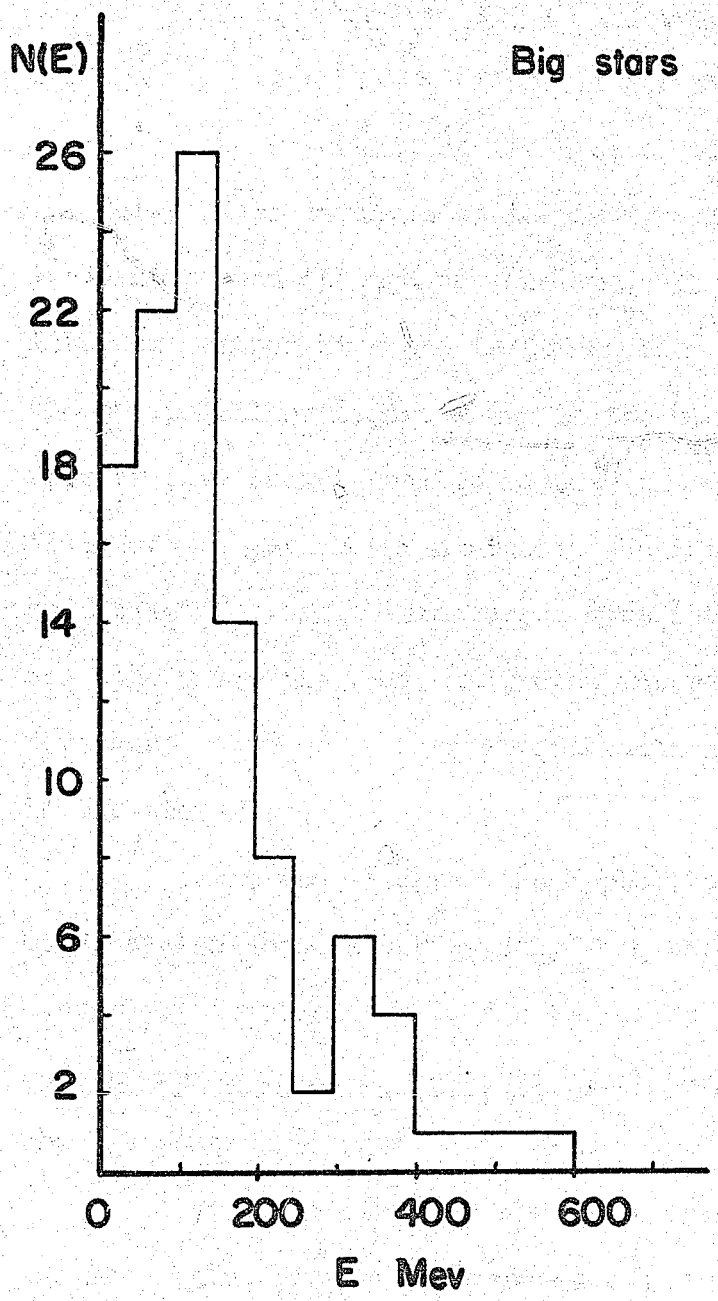

Fig. 26 - Energy spectrum of $\pi^{\pm}$ mesons

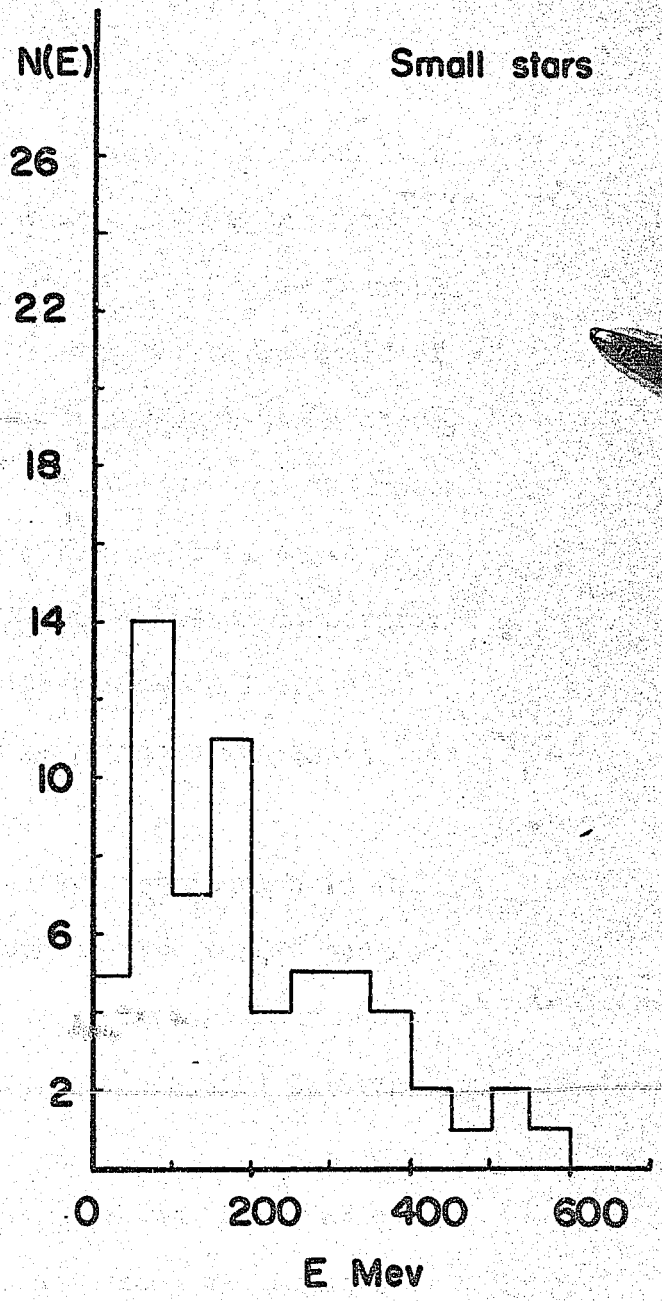

Fig. 27 - Energy spectrum of $\pi^{\pm}$ mesons

13. CONCLUSION

From the analysis of 51 small stars and 68 big stars, the mean meson multiplicity is found to be:

$$\langle \pi^{\pm} \rangle = 1.9 \pm .2 \text{ for small stars}$$

and

$$\langle \pi^{\pm} \rangle = 2.6 \pm .2 \text{ for big stars.}$$

The $\pi^{\pm}$-meson angular distribution of $\log(\cot\theta_L)$ indicates that the target mass involved in the interaction depends on the path of the incident proton through the nucleus. In small stars, the incident proton interacts either with one target nucleon mass or with the meson field of the peripheral nucleons, while in the big stars, it interacts with three, four or five target nucleon masses, one target nucleon mass and the meson field of the peripheral nucleons. Unfortunately the statistics are not sufficient to resolve the target mass into different π-meson masses for the case where the incident proton interacts with the meson field of the peripheral nucleons. Such an interaction is more prominent in small than in big stars.

From the study of the F-plot, the angular distribution in the C. M. system shows isotropy only when three, four or five target nucleon masses are involved, while for the cases where one target nucleon mass and the meson field of the peripheral target are involved, the distribution shows anisotropy.

From the study of the total transverse momentum distribution, the mean value of the transverse momenta of the $\pi^{\pm}$-mesons was found to to be:

$$\langle p_{\perp} \rangle = 0.59 \quad \mu c \quad \text{for small stars}$$

$$\langle p_{\perp} \rangle = 0.84 \quad \mu c \quad \text{for big stars.}$$

These values are lower than 1 μc, and the hydrodynamical model predicts it to be 1 μc. This deviation from the expected value may be explained by the small transverse momenta of the $\pi^{\pm}$-mesons produced by the interaction between the incident proton and the meson field of the peripheral nucleons, since such $\pi^{\pm}$-mesons are emitted at very small angles.

After removing those events in which the incident proton interacts with the meson field of the peripheral target nucleons, the mean value of the transverse momentum in the big stars becomes .90 μc.

Finally, the energy spectrum shows that there is a larger proportion of higher energy $\pi^{\pm}$-mesons in small than in big stars. This seems to be in agreement with the fact that the interaction between the incident proton and the meson field of the peripheral nucleons is more prominent in small than in big stars, as the $\pi^{\pm}$-mesons produced in such a process is of higher energy as compared with those due to a larger target mass interaction.

14. APPENDIX

As seen from the $\log(\cot\theta_L)$ distributions for the charged π-mesons in both small and big stars, different target nucleon masses are involved in the interaction. In addition to this, we observe the interaction of the incident proton and the meson field of the peripheral target nucleons. Due to the presence of this peripheral interaction, the assumption usually made that one-third of the π-mesons produced are π^o-mesons, is not valid. In the peripheral interaction, the target nucleon can either be a proton or a neutron. In the p-p peripheral interaction, a π^+-meson is most likely to be produced, while for the p-n peripheral interaction, the mode of interaction is not known at 6.2 Bev. Therefore, the proportion of π^o-mesons in the peripheral interaction cannot be estimated. For this reason the π-meson multiplicity is given only for the charged π-mesons.

BIBLIOGRAPHY

(1) Fermi, E., Prog. Theor. Phys., 5, 570 (1950)

(2) Hagedorn, R., Nuovo Cimento, 15, 434 (1960)

(3) Roesler, F.C. and McCusker, C.B.A., Nuovo Cimento, 10, 127 (1953)

(4) McCusker, C.B.A. and Roesler, F.C., Nuovo Cimento, 11, 98 (1954)

(5) Le Couteur, K.J., Proc. Phys. Society, A63, 259 (1950)

(6) Kalbach, R.M., Lord, J.J. and Tsao, C.H., Phys. Rev., 113, 330 (1959)

(7) Friedländer, E.M., Nuovo Cimento, 14, 796 (1959)

(8) Jain, P.L. and Glahe, H.C., Phys. Rev., 116, 458 (1959)

(9) Daniel, R.R., Kameswara Rao, N., Kalhotra, P.K. and Tsuzuki, Y., Nuovo Cimento, 16, 1 (1960)

(10) Winzeler, H., Klaiber, B., Koch, W., Nikolic, M. and Schneeberger, M, Nuovo Cimento, 17, 8 (1960)

(11) Bogachev, N.P., Bunyatov, S.A., Vishki, T., Yu. P. Merekov, Sidorov, V.M. and Yarba, V.A., Soviet Physics Jetp, 11, 317 (1960)

(12) Ali, H.H. and Fisher, C.M., Nuovo Cimento, 17, 98 (1960)

(13) Ancsin, J., Thesis, University of Ottawa (1960)

(14) Barbaro-Galtieri, A., Manfredini, A., Quassiati, B., Castagnoli, C, Gainotti, A., and Ortalli, Nuovo Cimento, 21, 469 (1961)

(15) Barashenkov, V.S., Baliakov, V.A., Glagolev, V.V., Dalkhazhav, N., Yao Tsyng-se, Kirillova, L.F.,Lebedev, R.M., Maltsev, V.M., Markov, P.K.,Shafranova, M.G., Tolstov, K.D., Tsyganov, E.N. and Wang Shou Feng, Nuclear Physics, 14, 522 (1959)

(16) Voyvodic, L. and Pickup, E., Phys. Rev., 85, 91 (1952)

(17) Castagnoli, C., Contini, G., Franzinetti, C., Manfredini, A., and Moreno, D., Nuovo Cimento, 10, 1539 (1953)

(18) Duller, N.M. and Walker, W.D., Phys. Rev., 93, 215 (1954)

(19) Bonsignori, F. and Selleri, F., Nuovo Cimento, 15, 465 (1960)

(20) Lindenbaun, S.J. and Sternheimer, R.M., Phys. Rev., 105, 1874 (1957)

(21) Barnes, V.E., Bugg, D.V., Dodd, W. P., Kinson, J.B. and Riddiford, L., Phys. Rev. letters, 7, 288 (1961)

(22) Melissinos, A.C., Fazio, G.G., Yamanouchi, T., Lindenbaun, S.J. and Yuan, L.C.L., Phys. Rev. Letters, 7, 454 (1961)

(23) Pickup, E., et al., Phys. Rev. Letters, 5, 161 (1960)

(24) Stonehill, D., Battay, C., Courant, H., Fickinger, W., Fowler, E.C., Kraybill, H., Sandweiss, J., Sanford, J.,and Taft, H., Phys. Rev. Letters, 6, 624 (1961)

(25) Milekhin, G.A. and Rosental', I.L., Soviet Physics Jetp, 6, 154 (1958)

(26) Zhdanov, G.B., Soviet Physics Jetp, 34, 592 (1958)